



# OPEN Integrative computational analysis of anti-influenza potential in *Caesalpinia mimosoides* Lamk hydroethanolic extract

Anuwachakij Klamrak<sup>1,12</sup>, Shaikh Shahinur Rahman<sup>1,2,12</sup>, Napapuch Nopkuesuk<sup>1</sup>, Jaran Nabnueangsap<sup>3</sup>, Jaraspim Narkpuk<sup>4</sup>, Piyapon Janpan<sup>1,5</sup>, Yutthakan Saengkun<sup>1,5</sup>, Thananya Soonkum<sup>3</sup>, Supawadee Sriburin<sup>1</sup>, Samaporn Teeravechyan<sup>4</sup>, Poramet Sitthiwong<sup>6</sup>, Nisachon Jangpromma<sup>5,7</sup>, Sirinan Kulchat<sup>8</sup>, Kiattawee Choowongkorn<sup>9</sup>, Rina Patramanon<sup>5,7</sup>, Arunrat Chaveerach<sup>10</sup>, Jureerut Daduang<sup>11</sup> & Sakda Daduang<sup>1,5</sup>✉

In a recent study, we used chemical analysis to show that the *Caesalpinia mimosoides* aqueous extract, which contains a high concentration of simple phenolics, has strong anti-influenza activity. We determined through molecular docking methods that its potential target inhibitor is the neuraminidase. Therefore, our study objectives were to evaluate whether the aqueous-ethanol extract (30% v/v) of this plant species exhibits greater antiviral activity than the aqueous plant extract. The *C. mimosoides* hydroethanolic extract exhibited potent antioxidant activity in the DPPH assay, with an  $IC_{50}$  value of 15.01  $\mu\text{g/mL}$ , comparable to authentic quercetin ( $IC_{50} = 12.72 \mu\text{g/mL}$ ) and approximately 4.91 times greater than standard gallic acid ( $IC_{50} = 3.06 \mu\text{g/mL}$ ). Through untargeted metabolomic analyses (UPLC-ESI(+)-QTOF-MS/MS) and subsequent stepwise computational metabolomics analyses, we identified the extract as primarily containing simple phenolics (e.g., gallic acid, ellagic acid, shikimic acid, and chlorogenic acid), flavonoid derivatives (e.g., quercetin, taxifolin, myricitrin, and afzelin), and other bioactive components, including dicarboxylic acids and germacrone. The polyphenol-rich extract showed strong anti-influenza activity, with an  $IC_{50}$  of 2.33  $\mu\text{g/mL}$  against the influenza A/PR/8/34 virus and no cytotoxic effects, as indicated by a  $CC_{50}$  greater than 50  $\mu\text{g/mL}$ . This represents an approximately 3.35-fold increase in effectiveness compared to its corresponding aqueous extract ( $IC_{50} = 7.81 \mu\text{g/mL}$ ). Furthermore, the extract demonstrated no hemolytic activity, even at a maximum concentration of 2,000  $\mu\text{g/mL}$ , suggesting its potential as a safe antiviral agent. Molecular docking analyses revealed that the identified phytochemicals can simultaneously interact with the “drug-target binding sites” of neuraminidase (NA) and PB2 subunit of influenza RNA polymerase, indicating their potential polypharmacological effects. The antiviral activity of the ethanolic-aqueous extract against other strains is being explored due to the versatile biological effects of phenolic substances.

**Keywords** *Caesalpinia mimosoides* Lamk, Anti-influenza, Hydroethanolic extract, Phytochemical profiling, Cheminformatics, Molecular docking

<sup>1</sup>Division of Pharmacognosy and Toxicology, Faculty of Pharmaceutical Sciences, Khon Kaen University, Khon Kaen 40002, Thailand. <sup>2</sup>Department of Applied Nutrition and Food Technology, Faculty of Biological Sciences, Islamic University, Kushtia 7000, Bangladesh. <sup>3</sup>Salaya Central Instrument Faculty RSPG, Research Management and Development Division, Mahidol University, Bangkok, Thailand. <sup>4</sup>Virology and Cell Technology Research Team, National Center for Genetic Engineering and Biotechnology (BIOTEC), National Science and Technology Development Agency (NSTDA), Pathumthani 12120, Thailand. <sup>5</sup>Protein and Proteomics Research Center for Commercial and Industrial Purposes (ProCCI), Khon Kaen University, Khon Kaen 40002, Thailand. <sup>6</sup>Khaoyai Panorama Farm Co., Ltd, 297 M.6, Thanarat Rd., Nongnamdang, Pakchong, Nakhonratchasima 30130, Thailand. <sup>7</sup>Department of Biochemistry, Faculty of Science, Khon Kaen University, Khon Kaen 40002, Thailand. <sup>8</sup>Department of Chemistry, Faculty of Science, Khon Kaen University, Khon Kaen 40002, Thailand. <sup>9</sup>Department of Biochemistry, Faculty of Sciences, Kasetsart University, Bangkok, Thailand. <sup>10</sup>Department of Biology, Faculty of Science, Khon Kaen University, Khon Kaen 40002, Thailand. <sup>11</sup>Department of Clinical Chemistry, Faculty of Associated Medical Sciences, Khon Kaen University, Khon Kaen 40002, Thailand. <sup>12</sup>Anuwachakij Klamrak and Shaikh Shahinur Rahman contributed equally to this work. ✉email: sakdad@kku.ac.th

Medicinal plants are valuable sources of phytochemicals that are utilized for the treatment of both infectious and non-infectious diseases<sup>1–3</sup>. Research studies have demonstrated the potential of plant extracts, particularly aqueous, ethanolic extract, and even hydroethanolic extract, as promising sources of antiviral agents, as they contain hydroxybenzoic acids, hydroxycinnamic acids, phenylpropanoids and terpenoids, which possess multiple-target actions disrupting various stages of viral life cycles, including attachment, entry, replication, spread, and even particle maturation<sup>4–7</sup>. An aqueous extract of *Toona sinensis*, for instance, primarily containing gallic acid and catechin, was found to disrupt multiple stages of the influenza virus (e.g., entry, spread, and replication) by concurrently targeting viral machinery proteins such as neuraminidase (NA), hemagglutinin (HA), and RNA polymerase<sup>7–9</sup>. Phenolic substances isolated from *Aronia melanocarpa*, including isoquercetin, kaempferol, ferulic acid, caffeic acid, ellagic acid, and myricetin, have been shown to inhibit the growth of influenza viruses, while also improving the survival rate of mice infected with the rPR8-GFP virus due to their antioxidant and anti-inflammatory properties<sup>10,11</sup>. These results prompt us to seek indigenous plants that can provide a diverse range of secondary metabolites as new, safe, affordable, and effective antiviral agents.

*Caesalpinia mimosoides* Lamk is a member of the Caesalpiniaceae family, where its young aerial parts, such as shoots and leaves, are commonly consumed as fresh or cooked vegetables in daily diets<sup>12</sup>. As per traditional medicine, it has also been used as a carminative to alleviate dizziness and fainting, indicating its potential therapeutic value and safety. Despite exhibiting various promising biological activities such as anticancer, antibacterial, antioxidant, anti-inflammatory, and neuroprotective effects<sup>13,14</sup>, research on the antiviral properties of medicinal plants in this family has been relatively limited. Although its virucidal effects need further exploration, our recent study demonstrates that the aqueous extract of *C. mimosoides*, primarily containing gallic acid and other shikimate-derived products (e.g., benzoic acid, quinic acid, shikimic acid, protocatechuic acid), can inhibit the influenza A/PR/8/34 virus with an impressive  $IC_{50}$  of 5.14  $\mu\text{g/mL}$  ( $CC_{50} > 100 \mu\text{g/mL}$ ) without inducing hemolytic effects on human red blood cells (hRBCs) at concentrations up to 800  $\mu\text{g/mL}$ <sup>15</sup>. Molecular docking studies also suggested that these compounds preferentially interacted with the oseltamivir recognition site and the 430-hydrophobic cavity of NA structure, thereby confirming the obtained results. Likewise, alcoholic extracts of *C. minax* and *C. latisiliqua*, both belonging to the same genus, have been found to exhibit significant antiviral activities due to the presence of flavonoids and stilbenes, whose  $IC_{50}$  values ranging from 5.09 to 12.20  $\mu\text{M}$ <sup>16</sup>. Owing to the potential of sharing an identical chemotaxonomic classification among the three plant species, there is growing interest in further developing *C. mimosoides* extracts with a myriad range of phytochemicals, ultimately acquiring more effective antiviral agents for pharmaceutical use.

High-resolution LC-MS/MS plays a crucial role in metabolomics analysis due to its exceptional capacity and sensitivity in detecting and tentatively identifying a wide range of metabolites in complex mixtures through untargeted analysis<sup>17,18</sup>. Several computational tools are developed for the structural annotation of natural products to enhance confidence levels in metabolite identification, primarily based on submitting raw mass spectra<sup>19,20</sup>. Of much software developed, SIRIUS, can derive the correct molecular formula of queried subjects mainly through the high-resolution isotopic pattern analysis<sup>21</sup>. Additionally, it is integrated with two essential tools, CSI: FingerID web service and CANOPUS, to provide more details about probable structures, substructures, and classifications of the query metabolites<sup>22</sup>. Using multiple software tools enables high-level structural annotation of bioactive constituents such as gallic acid, quinic acid, shikimic acid, pyrogallol, protocatechuic acid, bergenin, and various chain-length dicarboxylic acids found in the *C. mimosoides* aqueous extract<sup>15</sup>. Wang et al.<sup>23</sup> utilized computational tools to identify numerous phytochemicals in *Salvia miltiorrhiza* Bunge extract, identifying 34 tanshinones, 31 phenolics, and two new salvianolic acids for the first time via their untargeted metabolomics data<sup>24</sup>. This approach also enabled detailed structural annotation of 7 unknown and 17 known bioactive metabolites in the extract of *Urtica dioica* leaves<sup>25</sup>. For these reasons, it is thus crucial to adopt computational mass spectrometric approaches to structurally annotate bioactive constituents in the hydroethanolic extract of *C. mimosoides*, subsequently benefit in postulating precise antiviral mechanisms and identifying lead compounds for upcoming drug discovery programs. The objective of this study was to formulate a hydroethanolic extract of *C. mimosoides* utilizing leaves, stalks, and trunks (30% v/v ethanol solution). The study aimed to assess whether this solvent system would enhance the phytochemical profiling compared to the conventional aqueous extract. Additionally, the study evaluated the extract's antioxidant properties, identified gallic acid as a representative marker using HPLC analysis, and followed by untargeted metabolomics analysis (UPLC-ESI(±)-QTOF-MS/MS) to identify flavonoids and other active constituents such as terpenoids and alkaloids. The structural annotation of the deduced metabolites was performed using a comprehensive assessment of in-silico tools, including MetFrag, SIRIUS (v.5.6.8), CSI: FingerID, and CANOPUS, to achieve a high level of confidence in metabolite annotation (level 2), in accordance with metabolomics initiative guidelines<sup>26,27</sup>. As proposed earlier, we assessed the anti-influenza A/PR/8/34 virus and hemolytic activities of the hydroethanolic plant extract to ensure its efficacy and safety. Molecular docking against three viral machinery proteins, HA, NA, and PB2, was employed to elucidate the potential mechanisms responsible for antiviral activity.

## Materials and methods

### Preparation of *C. mimosoides* aqueous-ethanolic extract

Fresh aerial parts of *C. mimosoides*, including leaves and stalks, were harvested from an open field in Nam Phong subdistrict, Khon Kaen province, Thailand, at coordinates 16°37'59.9" north latitude and 102°46'14.3" east longitude. The harvested plant materials underwent thorough washing with tap water and double soaking in deionized water for 60 min each to ensure complete removal of any unwanted residues. Subsequently, they were dried at 50°C for 2–3 days using an oven incubator, ground, and milled into fine powder using a blender. A hydro-ethanolic extract was prepared by taking 20 g of plant material, placing it in a 500 mL Erlenmeyer flask, and extracting it with 200 mL of 30% v/v hydroethanolic solution. The extraction process involved gentle

shaking at 100 rpm and 25°C for 2 days to minimize the generation of reactive oxygen species (ROSs). The resulting mixture was then centrifuged at 8,000 rpm for 20 minutes at 25°C, producing a clear supernatant that was carefully transferred into a round-bottom flask. Approximately 100 mL of ethanol was evaporated using a BUCHI Rotavapor R-3 evaporator, followed by removal of the remaining water using a freeze dryer at -110°C (CoolSafe, Labogene, Lyngø, Denmark) for 48 hours. The freeze-dried extract was subsequently stored at -80°C until analysis.

### Total phenolic content (TPC)

Total phenolic content was determined using Folin and Ciocalteu (1927) method with some modifications<sup>28</sup> and the reaction took place in a 96-well plate. An aliquot (20 µL) of the extract, purified GA (1) and quercetin (> 95% purity Sigma-Aldrich, St. Louis MO, USA), or blank (deionized water) was carefully loaded into each well. After that, 100 µL of 0.2 M Folin–Ciocalteu reagent and 80 µL of 7% (w/v) sodium carbonate were added. Each set of samples was run in triplicate. The mixtures were incubated at 25 °C in constant darkness for 30 min before being analyzed using a microplate reader (EnSight Multimode Plate Reader, PerkinElmer, USA) at 760 nm. The presence of phenolics was calculated as gallic acid and quercetin equivalents (GAE) per gram of dry weight.

### DPPH assay

DPPH (2,2-diphenyl-1-picrylhydrazyl) assay was used to analyze the antioxidant property of the *C. mimosoides* hydroethanolic extract, as this property is closely associated with its antiviral activities. Gallic acid (Sigma-Aldrich, USA) and quercetin (Sigma-Aldrich, USA) were the reference standards DI water and absolute ethanol used as blank samples, respectively. Samples were mixed with 100 µL of 0.2 mM DPPH reagent, reactions were conducted in a dark environment for 30 min, and absorbance was measured at 517 nm using a microplate reader (EnSight Multimode Plate Reader). Results were expressed as IC<sub>50</sub> values and/or percentages of DPPH radical scavenging activity. The inhibition ratio (%) was calculated as follows:  $(A_{\text{control}} - A_{\text{sample}}) \times 100 / A_{\text{control}}$ , where  $A_{\text{control}}$  is the absorbance of the blank samples (DI water and ethanol), and  $A_{\text{sample}}$  is the absorbance of the reaction with the sample solution.

### HPLC analysis of gallic acid

Gallic acid was selected as a representative chemical marker due to its reported anti-influenza activity<sup>29</sup>. High-performance liquid chromatography with a diode-array detector (RP-HPLC-DAD) was employed to qualitatively and quantitatively analyze the presence of gallic acid in the *C. mimosoides* hydroethanolic extract. The analysis utilized an HPLC system from Agilent Technologies 1260 Infinity coupled with a PDA detector. Separation was achieved using a C-18 column (100 mm × 4.6 mm, 5 µm particle size, Phenomenex, USA). The mobile phases consisted of 0.5% phosphoric acid (solvent A) and methanol (solvent B). A linear gradient of solvent B was applied for metabolite separation, starting with 5% B for the first 2 min, increasing to 95% B over 15 min, holding at 95% B for 3 min, and returning to 5% B for the final 10 min, resulting in a total run time of 30 min at a flow rate of 0.8 mL/min. The sample and column temperatures were maintained at 25 °C, and detection was performed at 270 nm using a UV detector. Quantitative analysis was based on the five-point standard curve of gallic acid (62.5–1000 µg/mL) with the equation  $y = 68.215x + 1534.2$  ( $R^2 = 0.9976$ ).

### UPLC-ESI(±)-QTOF-MS/MS

Untargeted metabolomics analyses both negative and positive ion modes were implemented to gain full details of phenolics and non-phenolic compounds in the extract. An ultrahigh-performance liquid chromatograph (UHPLC) (UltiMate 3000 RSLCnano UHPLC System, Thermo Scientific, US), which is equipped with Acclaim<sup>®</sup> RSLC120 C18 (100 × 2.1 mm, 2.2 µm 120Å, Thermo Scientific, US) column were used in the separation processes. The 0.1% formic acid (solvent A) and acetonitrile (solvent B) were the mobile phases with a flow rate of 0.4 mL/min. A linear gradient of the solvent B as following conditions: 2% for 0–2 min, 0–90% for 1–12 min and hold for 2 min, and back to 2% for 4 min for a total run time of 18 min was implemented. The 1 µL of extract (final concentration of 10 ppm) was separated through the RP-column, where the temperature was maintained at 35 °C. The product identification of a mass spectrometer (TripleTOF6600+, AB SCIEX, Framingham, MA, USA) connected with the HPLC instrument. ESI source conditions were as follows: the ion source gas 1 50, ion source gas 2 60, curtain gas 30, a temperature of 150 °C, with the ion spray voltage floating of -4500 V in negative mode and 5500 V in positive mode. A TOF MS scan range of 100–800 amu. The product ion scan range of 50–800 Da. The scan accumulation time was 0.2 s, while the parent ion scan accumulation time was 0.25. The mass spectra were generated using a delustering potential (DP) of 80 V with the collision energy of 40 ± 10 eV. Metabolite matching was based on spectral similarity with the high-quality MS/MS spectrum deposited in the Natural Products HR-MS/MS library (version 2.0) and NIST 2017, which contains approximately 13,800 substances.

### Structural annotation using MetFrag webservice

The raw MS/MS spectra of selected metabolites from *C. mimosoides* aqueous-ethanolic extract were initially analyzed using MetFrag software (<https://msbi.ipb-halle.de/MetFrag/>) to obtain detailed information on the neutral formula, mass, and potential structure of the query metabolites. This process involves two steps: retrieving candidates and performing fragmentation setting and processing. First, a specific formula and corresponding  $m/z$  value must be provided, where various types of suspected databases to be selected to enhance annotation accuracy. In the case of metabolites originating from plant species, biological databases such as KEGG and NORMAN are strongly recommended<sup>30,31</sup>, as using the largest structural database (e.g., PubChem) lacks the capability to differentiate compounds possessing the same mass and chemical formula. After retrieving potential candidates, the experimental MS/MS data were matched against the in-silico generated spectra of these

candidates. Proposed compounds with an F score close to or equal to 1.0 were primarily considered potential candidates for the query subject.

### Metabolite annotation using SIRIUS (v.5.6.8)

The same raw mass dataset of selected metabolites was uploaded into the software. The MS2 level was set to a collision-induced dissociation (CID) energy of 30–50 eV, specifying the precursor ion (e.g.,  $m/z$  303.0522) and adduct type. Occasionally, the expected formula (e.g.,  $C_{15}H_{12}O_7$ ) was used to improve the precision of substance annotation. After clicking ‘compute’, SIRIUS, CSI: FingerID, and CANOPUS were selected to acquire more detailed information about natural products. Including biological databases like KEGG, NORMAN, PlantCyc, and Natural Products enhances the accuracy of metabolite annotation, especially when the query subjects are derived from natural resources.

### Anti-influenza virus screening assay

The influenza virus strain A/Puerto Rico/8/34 (H1N1) was used as a model to test the potential of a hydro-ethanolic plant extract to disrupt the viral cycle in a 96-well plate assay. MDCK cells were seeded at  $1.5 \times 10^5$  cells/well in serum-free OptiMEM (Invitrogen) with 2  $\mu\text{g/mL}$  TPCK-treated trypsin and incubated at 37 °C with 5%  $\text{CO}_2$  for 24 h. Assay involved mixing various concentrations of the extract (50–1.56  $\mu\text{g/mL}$ ) with viral particles (final concentration 100 pfu/well) at a 1:1 ratio at room temperature for 1 h. The virus-extract mixture was then added to MDCK cells, washed with PBS, and incubated for another 24 h. After fixing with ice-cold acetone, cells were blocked with PBST (PBS containing 0.5% Tween 20) and 2% BSA, followed by incubating with primary mouse anti-influenza A NP-UNLB antibody (BioLegend, 1:2000 dilution) and secondary HRP-conjugated goat anti-mouse antibody (BioLegend, 1:10,000 dilution). A colorimetric assay with TMB (3,3',5,5'-Tetramethylbenzidine) substrate was conducted at room temperature for 8 min, and absorbance at 450 nm was measured using a microplate reader. Prior to antiviral testing, cytotoxicity was assessed using the MTT assay across a range of extract concentrations (100 to 0.05  $\mu\text{g/mL}$ ) to ensure safety and distinguish between extract effects on cell viability and its antiviral activity.

### Hemolytic activity assay

Hemolytic activity of the *C. mimosoides* hydroethanolic extract was evaluated using human red blood cells (hRBCs) as described in our recent publication<sup>15</sup>. The study protocol was approved by the Ethics Committee of the Faculty of Biological Sciences, Islamic University, Kushtia, Bangladesh (Approval No. ERC/FBS/I.U./2022/09). Written informed consent was obtained from the participant before blood collection, and all experiments followed the guidelines and regulations of the Declaration of Helsinki. Briefly, hRBCs were resuspended in PBS (pH 7.4) at a final concentration of 4% (v/v). Due to the fragile nature of hRBCs, the suspension was carefully transferred to a new tube, mixed with 10  $\mu\text{L}$  of the plant extract, and incubated at 37 °C for 60 min. Clear supernatants were obtained by centrifugation at 10,000x g for 5 min and immediately transferred into a 96-well plate before measuring the signal intensity at 415 nm. Hemolytic activity was calculated using the equation: % hemolysis =  $(S/P) \times 100$ , where S represents the absorbance of the samples and P represents the absorbance of the positive control (0.1% Triton X-100). Hemolytic activity of less than 15% indicates a promising safety profile for human use<sup>32</sup>.

### Molecular docking

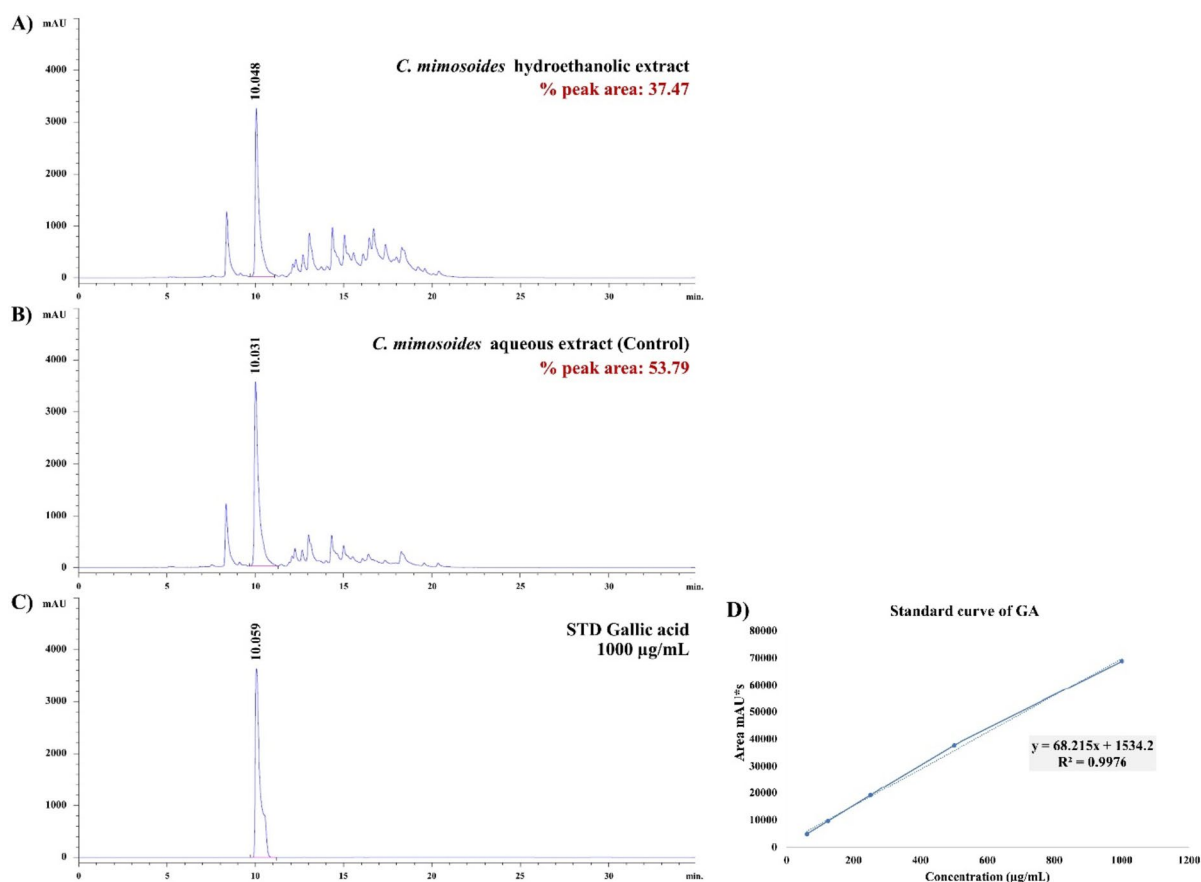
The docking study aimed to elucidate the mechanisms underlying the potent antiviral activity of various phytochemicals from the *C. mimosoides* hydroethanolic extract. Hemagglutinin (HA) and neuraminidase (NA) play crucial roles in the entry and spread of influenza viruses<sup>33</sup>. Crystal structures of influenza A (H1N1) HA (1RU7; resolution 2.30 Å) and NA (6HP0; resolution: 1.88 Å) were obtained from the Protein Data Bank (PDB). The NA structure is co-crystallized with GJT ((3R,4R,5 S)-4-acetamido-5-[4-(hydroxymethyl)triazol-1-yl]-3-pentan-3-yloxycyclohexene-1-carboxylic acid; PubChem CID: 139030257), enabling establishment of an accurate RMSD (Root Mean Square Deviation) value using GOLD (Genetic Optimization of Ligand Docking) docking software (v.5.2.2). HA, however, lacks co-crystallized ligands. CB-DOCK2 (<https://cadd.labshare.cn/cb-dock2/php/index.php>), a cavity-based docking tool, was used to identify an appropriate binding pose, using sialic acid as the natural substrate. Subsequently, Self-docking was performed for both the HA/sialic acid and NA/GJT complexes to confirm that their RMSD values were below 2.0 Å, ensuring a highly reliable docking pose. HA and NA achieved RMSD values of 1.2912 and 1.3602 Å, respectively. For the last viral protein model which is influenza polymerase basic protein 2 (PB2, PDB: 4NCE) with an RMSD of 1.7851, it was also included in the study. The Swiss PDB Viewer (v.4.1.0) was employed to replace missing residues in NA and PB2 prior to docking experiments.

## Results and discussion

### Total phenolic content (TPC) and radical scavenging activity assays

Evidence indicates a significant link between phenolic substances found in specific plant extracts and their antiviral capabilities, as they found to interact with active sites of viral proteins (e.g., NA, HA, and PB2), forming strong hydrogen bonds and hydrophobic interactions<sup>15,29,34,35</sup>. Assessment of TPC and radical scavenging activity is a primary concern. TPC value of hydroethanolic plant extract was 337 (GAE)/g DE. As measured by the DPPH assay, its  $\text{IC}_{50}$  value of 15.01  $\mu\text{g/mL}$ , highly resembling to the authentic quercetin ( $\text{IC}_{50}$  = 12.72  $\mu\text{g/mL}$ ) and approximately 4.91 times higher than that of standard gallic acid ( $\text{IC}_{50}$  = 3.06  $\mu\text{g/mL}$ ) (Table 1). This indicated its potential as a source of phytochemicals, where the chemical details must be unraveled to fully understand the mechanisms underlying its antiviral properties, shedding light on its future uses.

Sample	(DPPH assay) IC <sub>50</sub> µg/mL
<i>C. mimosoides</i> hydroethanolic extract	15.01
<i>C. mimosoides</i> aqueous extract (control)	12.05
Quercetin	12.72
Gallic acid	3.06
Total phenolic content (TPC)	
<i>C. mimosoides</i> hydroethanolic extract	337 mg (GAE)/g DE

**Table 1.** Radical scavenging property of various samples.**Fig. 1.** HPLC analysis of gallic acid as representative marker. (A) 30% hydroethanolic extract. (B) Aqueous extract. (C) standard gallic acid (1 mg/mL). (D) Standard curve of gallic acid.

### HPLC analysis of gallic acid in *C. mimosoides* hydroethanolic extract

Drawing from our previous conclusions, gallic acid is one of the major constituents typically detected in *C. mimosoides* extracts (e.g., water, methanol, ethanol, ethyl acetate, and hexane)<sup>15</sup>. It is proposed to be involved in the anti-influenza activities of various plant extracts<sup>36</sup>. Hence, this compound served as a representative marker for the quality control of the *C. mimosoides* aqueous ethanolic extract detailed here. As expected, a peak (Rt = 10.048 min) matching the authentic gallic acid (Rt = 10.072 min) was found in the 30% hydroethanolic extract (Fig. 1). Based on comparison with the five-point calibration curve ( $R^2 = 0.9976$ ), the yield of gallic acid was found to be 7.12 mg/g DW (dried weight) of plant material, which was lower than that detected in the *C. mimosoides* aqueous extract (8.77 mg/g DW) (Table 2). Since the gallic acid peak comprises 37.47% of the relative peak area, the remaining substances (approximately 62.53%) need to be explored to gain insight into other polyphenols and compounds present in the extract that may synergistically govern antioxidant and anti-influenza properties.

### Metabolic profiling and structural annotation of metabolites using cheminformatics tools

The untargeted metabolomics analysis tentatively identified forty-eight bioactive metabolites in the hydroethanolic extract of *C. mimosoides* (Table 3). They exhibited reliable matching library scores ranging from 71.4 to 100% (with a mass error of < 20 ppm), though some deviated from these criteria. They were additionally



Sample	Yield of gallic acid (mg/g, dried weight)
Hydroethanolic extract (30% v/v)	7.12
Aqueous extract	8.77

**Table 2.** Quantitative analysis of gallic acid in *C. mimosoides* extracts using HPLC technique.




annotated using a series of in-silico tools to detail regarding the correct molecular formula, candidate structure, substructure, and even compound class, achieving a high level of confidence in metabolite annotation (level-2). Upon stepwise examination using the MetFrag and SIRIUS, 35 out of 48 metabolites could be annotated as top-ranked candidates (1st and 2nd level structural reliability) among hundreds of potential structures retrieved from biological databases, gratifying the metabolomics initiative guidelines<sup>20,22</sup>. According to compound classification by CANOPUS (Class Assignment and Ontology Prediction Using Mass Spectrometry), they were simple phenolics, flavonoids with glycoside derivatives, carboxylic acids, terpenoids, and alkaloids, highlighting the remarkable structural diversity of the newly prepared extract and strengthening our supposition that *C. mimosoides* could be a promising source of natural antiviral agents, particularly shikimate- and phenylpropanoid-derived natural products, similar to *C. minax* and *C. latisiliqua*<sup>16</sup>. Notably, the correctness of structural annotation of all detected flavonoids (e.g., quercetin, quercitrin, and taxifolin) is likely confirmed by the presence of *p*-coumaric acid (*m/z* 163.0411), which is known to be subsequently metabolized by 4-coumarate CoA-ligase (4CL), chalcone synthase (CHS), and chalcone isomerase (CHI) to produce naringenin, a key branching point in the biosynthesis of flavonoids widely distributed in the plant kingdom<sup>28</sup>. Meanwhile, the detection of negative ion of gallic acid (*m/z* 169.0178) and its related metabolites, including ethyl gallate (*m/z* 197.0522), pyrogallol (*m/z* 125.0270), shikimic acid (*m/z* 173.0485), quinic acid (*m/z* 191.0651), ellagic acid (*m/z* 300.9999), and chlorogenic acid (*m/z* 353.0910) as top candidates (1st), supports a previous study showing that they originated from the shikimic route<sup>37</sup>, thus validating their reliability for structural annotation. The putative pyrogallol (*Rt* = 2.16 min), with a lower relative peak area (9.16%), was identified as co-eluting with gallic acid (29.64%: *Rt* = 2.16 min), suggesting they share similar physicochemical features and biosynthetic pathways. Although untargeted metabolomics on phenolic-rich extracts are often more effective in negative ion mode<sup>38</sup>, the use of positive ion mode confirmed various flavonoids, including myricetin, guaijaverin, (-)-galocatechin, quinic acid, quercetin, luteolin 7-glucuronide, and afzelin, which formerly detected in the negative ionization. Notably, astragalin and luteolin 7-glucuronide, tentatively characterized by *m/z* 449.1102 and *m/z* 463.0890 respectively, could also be detected exclusively. An increase in the ethanol concentration to 30% v/v in the extract solvent enabled the detection of putative germacrone (*m/z* 463.0890), because of its hydrophobic properties. Unfortunately, the remaining 13 metabolites had to be classified as ‘improper structures; N.D.’ because neither MetFrag nor SIRIUS could annotate them as previously explained by the MS/MS-libraries, resulting in low-confidence identification. Potential factors contributing to these inconsistencies likely include inadequate collision-induced energies, significant mass errors (>20 ppm), and misidentification due to deficiencies within the spectral libraries<sup>26</sup>. The examples of metabolites successfully annotated by SIRIUS, in tandem with the connected tools, classified by compound classification, are as follows:

#### Ellagic acid

Of the ten proposed formulas, high-resolution isotope pattern analysis confirmed that the query metabolite at *m/z* 300.9999 has the formula  $C_{14}H_6O_8$  (Fig. 2), conforming with the entry in the database (<https://pubchem.ncbi.nlm.nih.gov/compound/Ellagic-Acid>). By comparing against biological databases, CSI: FingerID subsequently identified this natural substance as ellagic acid (1st), presumably due to the pre-existing in the training dataset. Numerous substructures illustrating the successive dimerization of gallic acids followed by cyclization were also detected in the most potential candidate, such as “[#6]c1c([#8])cccc1 (Cc1c(O)ccc1 (gallic acid))”, “[#8]=:[#6]-,[#6]-,[#6]-,[#6]-,[#6]-,[#6] (O=C-C-C-C-C(O)-C) (another gallic acid)”, “[#8]=:[#6]-,[#6]-,[#6]-,[#6]-,[#6]-,[#6]=:[#8] (O=C-C-C-C-C=O) (cyclized region)”, and “c(:c: c:o): c:1 (ring closure unit)”. Of equal importance, substructures that indicated the successive formation of ellagic acid, described by “c(:c: c:c(c1)c(:c(:c: c:c2)~[!#1]): c2~[!#1]): c1” and “c(:c(:c(:c: c1):o: c:c2):c2):c:1 (coumarin-like structure)” were also detected. This query subject exhibited a mass fragmentation pattern highly similar to that of authentic ellagic acid established by Yan et al.<sup>39</sup>, characterized by the product ions with *m/z* values of 185.026, 229.0157, 257.0106, and 283.998. They were suggested to the same substance. CANOPUS also affirmed that gallotannins, phenol acids ( $C_6-C_1$ ), and shikimates & phenylpropanoids were the class, superclass, and biosynthetic origin of this natural product, respectively.

#### Chlorogenic acid

Among the one hundred potential metabolites retrieved from Biodatabases, the negative precursor ion at *m/z* 353.091 was best annotated as chlorogenic acid (1st), owing to its pre-inclusion in the CSI: FingerID structure training set (<https://www.csi-fingerid.uni-jena.de/v2.6/api/fingerid/trainingstructures?predictor=2>). Numerous fingerprints illustrating the successive ester bond formation between quinic acid and caffeic acid to yield chlorogenic acid were found in the query subject. For instance, substructures encoded by “C(CC(CC-1~[#8])~[#8])(C-1~[#8]~[#8]); (100%)” and “[#8]c1c([#8])cccc1 (Oc1c(O)cccc1); (98%)”, signifying the presence of quinic acid and caffeic acid, respectively. Meanwhile, the ester bonds (R-COO-R’) formed by the two phenolic substances, ‘ECFP6: 1639092370 (100%)’ and ‘ECFP6: 169346356 (100%)’, were detected in the same structural candidate (Fig. 3). The fragment ions at *m/z* 191.0585 (base peak) and *m/z* 179.0358 emerged




UPLC-ESI(±)-QTOF-MS/MS													
No.	Retention time (min)	Proposed phytochemical (% relative peak area)	Correct neutral formula (SIRIUS score %)	Neutral mass	Theoretical (m/z) [M-H] <sup>+</sup> / [M+H] <sup>+</sup>	Exp. mass (m/z)	Mass error (ppm)	Library score (%)	Rank/DB (F1 Score)	Rank/DB (CSI: Fingerprint Training (YES/NO))	Lipophilicity Log <i>P</i> <sub>ow</sub> (iLOGP)		
1	5.84	Taxifolin (0.04)	C <sub>15</sub> H <sub>10</sub> O <sub>7</sub> (99.998)	304.06	303.0505	303.0522	5.61	72.5	2nd /NORMAN (0.9017)	1st /Bio databases (100) (Yes)	1.30		
2	5.11	Quercetagetin-7-O glucoside (0.41)	C <sub>21</sub> H <sub>20</sub> O <sub>13</sub> (97.066)	480.09	479.0826	479.0854	5.84	96.6	N.D.	2st / PlantCyc (82.74) (Yes)	1.68		
3	6.76	Myricetin (0.06)	C <sub>15</sub> H <sub>10</sub> O <sub>8</sub> (99.224)	318.04	317.0297	317.0314	5.36	99.2	2nd /NORMAN (0.9645)	1st /Bio databases (Yes)	1.08		
4	6.27	Quercitrin (7.01)	C <sub>21</sub> H <sub>20</sub> O <sub>11</sub> (99.51)	448.10	447.0927	447.1026	22.14	98.9	1st /NORMAN (1.0)	1st /Bio databases (100) (Yes)	1.27		
5	5.76	Ellagic acid (0.07)	C <sub>14</sub> H <sub>6</sub> O <sub>8</sub> (100)	302.01	300.9984	300.9999	4.98	94.5	1st /NORMAN (1.0)	1st /Bio databases (100) (Yes)	0.79		
6	4.29	Esculetin (0.13)	C <sub>9</sub> H <sub>6</sub> O <sub>4</sub> (100)	178.03	177.0188	177.0200	6.78	94.1	2nd /KEGG (0.8163)	1st /Bio databases (99.49) (Yes)	1.25		
7	3.79	Chlorogenic Acid (0.91)	C <sub>16</sub> H <sub>18</sub> O <sub>9</sub> (99.703)	354.10	353.0873	353.0910	10.48	100	1st /NORMAN (1.0)	1st /Bio databases (100) (Yes)	0.96		
8	8.63	2-Methylcinnamic acid (0.02)	–	162.07	161.0603	161.0360	–150.88	83.9	N.D.	N.D.	1.70		
9	3.6	4-Methylcinnamic acid (0.10)	–	162.07	161.0603	161.0825	137.84	54.9	N.D.	N.D.	1.79		
10	5.47	<i>p</i> -coumaric acid (0.65)	C <sub>9</sub> H <sub>8</sub> O <sub>3</sub> (99.998)	164.05	163.0395	163.0411	9.81	97.3	3rd /NORMAN (0.9999)	1st /EcoCyc Mine (86.71) (Yes)	0.95		
11	0.84	Maleic acid (0.20)	–	116.01	115.0031	115.0042	9.56	99.6	N.D.	N.D.	0.32		
12	6.08	Scutellarin (0.11)	C <sub>21</sub> H <sub>18</sub> O <sub>12</sub> (98.567)	462.08	461.0720	461.0739	4.12	98.9	1st /NORMAN (1.0)	1st /NORMAN (78.33) (Yes)	1.11		
13	5.44	Limonin (0.12)	–	470.19	469.1862	469.1768	–20.03	82.9	N.D.	N.D.	2.87		
14	4.74	Dihydromyricetin (0.11)	C <sub>15</sub> H <sub>12</sub> O <sub>8</sub> (100)	320.05	319.0454	319.0467	4.07	96.3	2nd /KEGG (0.9592)	1st /Bio databases (100) (Yes)	0.90		
15	5.14	Asiatic acid (0.18)	–	488.35	487.3424	487.3071	–72.43	56.8	N.D.	N.D.	3.20		
16	0.73	Daidzin [M+FA-H] <sup>–</sup> (0.04)	C <sub>21</sub> H <sub>20</sub> O <sub>9</sub> (N.D.)	416.11	461.1084	461.1522	94.99	57.6	2nd /NORMAN (0.9162)	N.D.	1.77		
17	6.04	2,6-Dihydroxy-4-methylbenzoic acid (0.06)	C <sub>8</sub> H <sub>8</sub> O <sub>4</sub> (100)	168.04	167.0344	167.0355	6.59	61.6	N.D.	2nd /Bio databases (100) (Yes)	0.90		
Continued													

UPLC-ESI(±)-QTOF-MS/MS											
No.	Retention time (min)	Proposed phytochemical (% relative peak area)	Correct neutral formula (SIRIUS score %)	Neutral mass	Theoretical (m/z) [M-H] <sup>-</sup> /[M + H] <sup>+</sup>	Exp. mass (m/z)	Mass error (ppm)	Library score (%)	Rank/DB (F1 Score)	Rank/DB (CSI: Fingerprint Matching Score%) Training (YES/NO)	Lipophilicity Log <i>P</i> <sub>ov</sub> (iLOGP)
18	8.75	Undecanedioic acid (0.13)	C <sub>11</sub> H <sub>20</sub> O <sub>4</sub> (100)	216.14	215.1283	215.1303	9.30	93.2	1st /LipidMaps (1.0)	1st /Bio databases (100) (Yes)	1.92
19	5.22	Ethyl gallate (0.05)	C <sub>9</sub> H <sub>10</sub> O <sub>5</sub> (98.966)	198.05	197.0450	197.0522	36.54	83.3	3rd /NORMAN (0.9598)	1st /Bio databases (99.50%) (Yes)	1.21
20	11.23	Tetradecanedioic acid (0.17)	C <sub>14</sub> H <sub>26</sub> O <sub>4</sub> (100)	258.18	257.1753	257.1776	8.94	99.9	1st /LipidMaps (0.0)	1st /Bio databases (100) (Yes)	2.49
21	12.4	Hexadecanedioic acid (0.06)	C <sub>16</sub> H <sub>30</sub> O <sub>4</sub> (100)	286.21	285.2066	285.2084	6.31	99.9	2nd /LipidMaps (1.0)	1st /Bio databases (100) (Yes)	2.98
22	3.95	Catechin (0.97)	C <sub>15</sub> H <sub>14</sub> O <sub>6</sub> (100)	290.08	289.0712	289.0752	13.84	97	1st /NORMAN (1.0)	1st /Bio databases (100) (Yes)	1.47
23	0.91	Shikimic acid (33.24)	C <sub>7</sub> H <sub>10</sub> O <sub>5</sub> (100)	174.05	173.0450	173.0485	20.23	90.9	1st /NORMAN (0.7683)	1st /NORMAN (100) (Yes)	0.45
24	6.59	Azelaic acid (0.40)	C <sub>9</sub> H <sub>16</sub> O <sub>4</sub> (100)	188.10	187.0970	187.0993	12.29	90.8	2nd /LipidMaps (0.9499)	1st /Bio databases (100) (Yes)	1.44
25	2.16	Pyrogallol (9.16)	C <sub>6</sub> H <sub>6</sub> O <sub>3</sub> (100)	126.03	125.0239	125.0270	24.80	99.8	8th /NORMAN (0.7634)	1st /Bio databases (Yes) (91.74)	0.97
26	0.8	myo-Inositol (0.84)	C <sub>6</sub> H <sub>12</sub> O <sub>6</sub> (100)	180.06	179.0556	179.0567	6.14	73.7	1st /KEGG (0.4076)	1st /Bio databases (93.83) (Yes)	0.31
27	18.37	Malonic acid (0.03)	–	104.01	103.0031	102.9711	–310.67	77.3	N.D.	N.D. (No)	–0.08
28	2.16	Gallic acid (29.64)	C <sub>7</sub> H <sub>6</sub> O <sub>5</sub> (100)	170.02	169.0137	169.0178	24.26	97.5	1st /KEGG (1.0)	1st /Bio databases (97.69) (Yes)	0.21
Continued											



UPLC-ESI(±)-QTOF-MS/MS											
No.	Retention time (min)	Proposed phytochemical (% relative peak area)	Correct neutral formula (SIRIUS score %)	Neutral mass	Theoretical (m/z) [M-H] <sup>+</sup> / [M+H] <sup>+</sup>	Exp. mass (m/z)	Mass error (ppm)	Library score (%)	Rank/DB (F1 Score)	Rank/DB (CSI; FingerID Matching Score%) Training (YES/NO)	Lipophilicity Log P <sub>ow</sub> (iLOGP)
29	0.95	4-Hydroxybenzoic acid (2.64)	C <sub>7</sub> H <sub>6</sub> O <sub>3</sub> (100)	138.03	137.0239	137.0247	5.84	100	1st /KEGG (1.0)	1st /Bio databases (97.90) (Yes)	0.85
30	13.17	Heptadecanoic acid (0.56)	–	270.26	269.2481	269.2142	–125.91	92.1	N.D.	N.D. (No)	4.11
31	6.04	Guaijaverin (0.33)	C <sub>20</sub> H <sub>18</sub> O <sub>11</sub> (99.771)	434.08	433.0771	433.0794	5.31	99	1st /NORMAN (1.0)	1st /Bio databases (99.68) (Yes)	1.61
32	5.44	Myricitrin (1.01)	C <sub>21</sub> H <sub>20</sub> O <sub>12</sub> (100)	464.10	463.0877	463.2196	284.83	79.2	1st /NORMAN (1.0)	1st /Bio databases (92.12) (Yes)	0.92
33	2.97	(-)-Gallicocatechin (0.36)	C <sub>15</sub> H <sub>14</sub> O <sub>7</sub> (99.995)	306.07	305.0661	305.0681	6.56	90.2	1st /NORMAN (1.0)	1st /Bio databases (100) (Yes)	0.98
34	0.76	Quinic acid (5.83)	C <sub>7</sub> H <sub>12</sub> O <sub>6</sub> (100)	192.06	191.0556	191.0651	49.72	95.8	1st /KEGG (1.0)	1st /Bio databases (98.72) (Yes)	–0.12
35	7.7	Quercetin (0.02)	C <sub>15</sub> H <sub>10</sub> O <sub>7</sub> (100)	302.04	301.0348	301.0364	5.32	94.8	1st /NORMAN (1.0)	1st /Bio databases (100) (Yes)	1.63
36	6.85	Afzelin (4.35)	C <sub>21</sub> H <sub>20</sub> O <sub>10</sub> (100)	432.11	431.0978	431.1052	17.17	100	1st /KEGG (1.0)	1st /Bio databases (100) (Yes)	1.8
37	5.6	Myricetin (17.81)	C <sub>15</sub> H <sub>10</sub> O <sub>8</sub> (99.224)	318.04	319.0454	319.0488	10.66	90	1st /KEGG (1.0)	1st /Bio database (97.30) (Yes)	1.08
38	0.73	Hamaudol Glycoside (0.87)	–	438.15	439.1604	439.1438	–37.80	77.8	ND.	N.D. (No)	2.75
39	6.07	Guaijaverin (0.88)	C <sub>20</sub> H <sub>18</sub> O <sub>11</sub> (N.D.)	434.08	435.0927	435.0946	4.37	98.4	1st /NORMAN (1.0)	N.D. (No)	1.61
40	8.57	Germacone (0.51)	C <sub>15</sub> H <sub>22</sub> O (100)	218.17	219.1749	219.1393	–162.43	88	8th /KEGG (0.8698)	1st /MesH, PubMed, Zinc Databases (67.72) (Yes)	2.96
Continued											

UPLC-ESI(±)-QTOF-MS/MS												
No.	Retention time (min)	Proposed phytochemical (%) relative peak area	Correct neutral formula (SIRIUS score %)	Neutral mass	Theoretical (m/z) [M-H] <sup>+</sup> / [M+H] <sup>+</sup>	Exp. mass (m/z)	Mass error (ppm)	Library score (%)	Rank/DB (F1 Score)	Met:rag	SIRIUS	Lipophilicity Log P <sub>ow</sub> (iLOGP)
41	4.48	Bergamottin (3.50)	C <sub>21</sub> H <sub>32</sub> O <sub>4</sub> (N.D.)	338.15	339.1596	339.1101	-145.95	53.9	8th / ChEBI (0.531)		N.D. (No)	4.02
42	7.71	(E)-beta-Damascone (1.97)	C <sub>13</sub> H <sub>20</sub> O (100)	192.151	193.1592	193.1602	5.18	94.6	N.D.		1st /Additional database (Yes)	2.83
43	0.72	D-Pinitol (1.23)	C <sub>7</sub> H <sub>14</sub> O <sub>6</sub> (100)	194.08	195.0869	195.0884	7.69	90	1st /KEGG (1.0)		1st /Bio database (Yes)	0.36
44	0.82	Stachydrine (2.38)	-	143.09	144.1025	144.1035	6.94	98.5	N.D.		N.D. (No)	-1.20
45	0.7	Emodin-8-glucoside (3.37)	C <sub>21</sub> H <sub>30</sub> O <sub>10</sub> (N.D.)	432.11	455.0954	455.1185	50.76	78.6	3 out of 545/ PubChem (0.0)		N.D. (No)	1.55
46	5.56	Loganic acid (1.40)	C <sub>6</sub> H <sub>14</sub> O <sub>6</sub> (N.D.)	376.14	399.1267	399.1436	42.34	62.2	1st /NORMAN (1.0)		N.D. (No)	1.26
47	2.96	(-)-Galocatechin (0.49)	C <sub>15</sub> H <sub>14</sub> O <sub>7</sub> (100)	306.07	307.0818	307.0836	5.86	96.6	1st /KEGG (1.0)		1st/Bio databases (Yes)	0.98
48	6.74	Citronellic acid (1.95)	C <sub>10</sub> H <sub>18</sub> O <sub>2</sub> (N.D)	170.13	171.1385	171.1506	70.70	73.1	5th /KEGG (0.7608)		N.D. (No)	2.28
49	13.43	6-Methylcoumarin (1.16)	-	160.05	161.0603	161.0970	227.86	51.4	N.D.		N.D. (No)	2.03
50	0.78	Trigonelline (40.95)	C <sub>7</sub> H <sub>7</sub> NO <sub>2</sub> (100)	137.05	138.0555	138.0572	12.31	98.1	2nd /KEGG (1.0)		1st/ Bio databases (93.79) (Yes)	-3.11
51	0.76	Quinic acid (3.75)	C <sub>7</sub> H <sub>12</sub> O <sub>6</sub> (100)	192.06	193.0712	193.0729	8.81	63.9	3rd/KEGG (1.0)		1st/Bio databases (69.70) (Yes)	-0.12
52	6.28	Astragalin (9.00)	C <sub>21</sub> H <sub>20</sub> O <sub>11</sub> (100)	448.10	449.1084	449.1102	4.01	100	N.D.		1st/Bio databases (91.59) (Yes)	0.53
53	6.11	Luteolin 7-glucuronide (1.09)	C <sub>21</sub> H <sub>18</sub> O <sub>12</sub> (100)	462.08	463.0877	463.0890	2.81	71.4	1st/KEGG (1.0)		1st/BioCyc (79.10) (Yes)	1.55
continued												

No.	UPLC-ESI(±)-QTOF-MS/MS										
	Retention time (min)	Proposed phytochemical (% relative peak area)	Correct neutral formula (SIRIUS score %)	Neutral mass	Theoretical (m/z) [M-H] <sup>-</sup> / [M+H] <sup>+</sup>	Exp. mass (m/z)	Mass error (ppm)	Library score (%)	Rank/DB (F1 Score)	Rank/DB (CSI: FingerID Matching Score%) Training (YES/NO)	Lipophilicity Log P <sub>ow</sub> (iLOGP)
54	6.28	Quercetin (1.59)	C <sub>15</sub> H <sub>10</sub> O <sub>7</sub> (100)	302.04	303.0505	303.0529	7.92	99.8	3rd/NORMAN (0.9116)	1st/Bio databases (100) (Yes)	1.63
55	6.87	Afzelin (6.11)	C <sub>21</sub> H <sub>30</sub> O <sub>10</sub> (100)	432.11	433.1135	433.157	5.08	100	2nd/KEGG (0.995)	1st/Bio databases (99.68) (Yes)	1.84

**Table 3.** Molecular formula and rank annotation of bioactive metabolites present in the hydroethanolic extract of *C. mimosoides* using UPLC-ESI(±)-QTOF-MS/MS coupled with Sirius (v5.8.6) and MetFrag webservice.

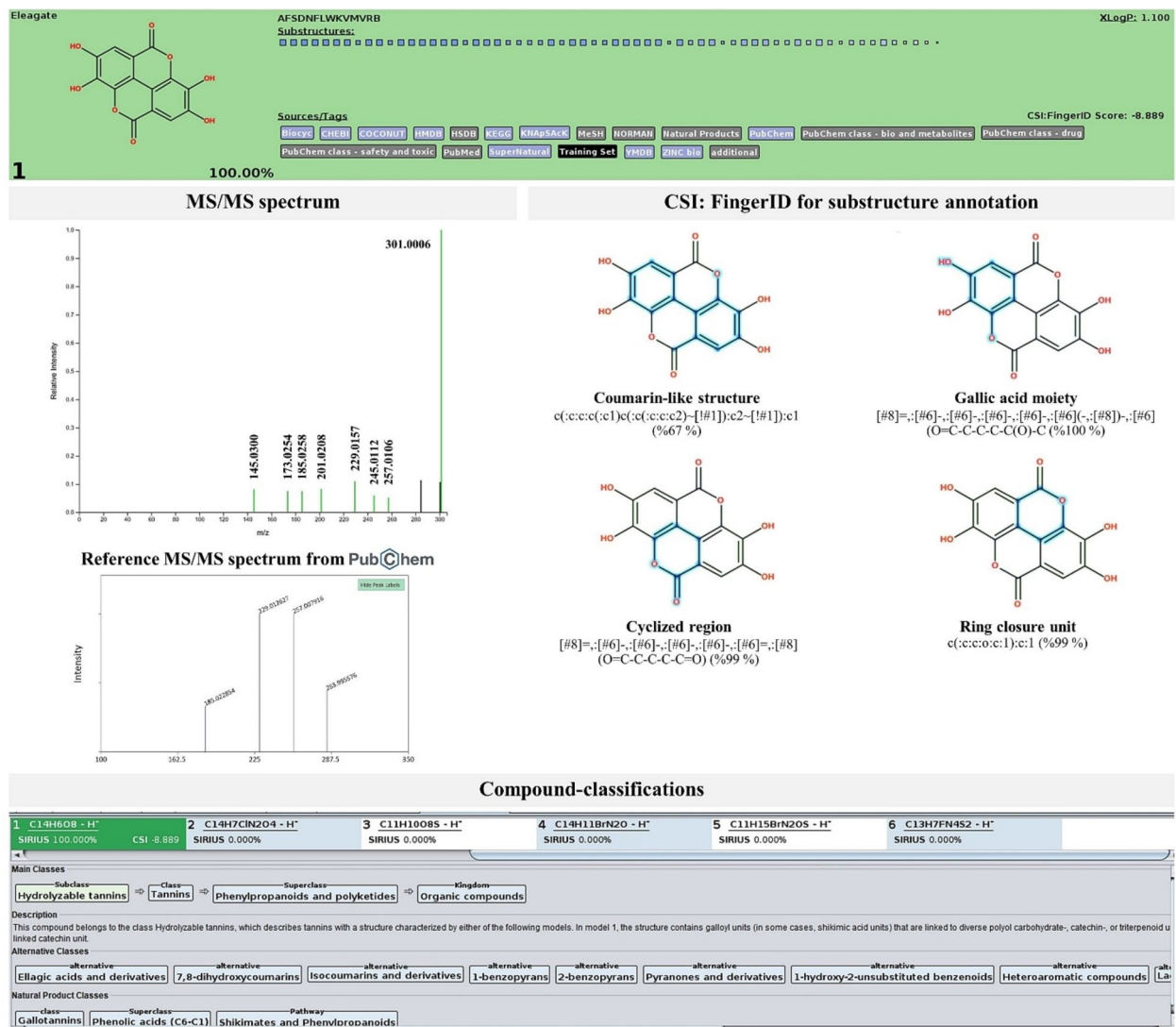


**Fig. 2.** Structural annotation of putative ellagic acid.

in the MS/MS spectrum indicate the consecutive loss of quinic acid from the caffeic moiety, conforming to its authentic structure in PubChem (<https://pubchem.ncbi.nlm.nih.gov/compound/Chlorogenic-Acid#section=Computed-Properties>). Compound classifications show that cinnamic acids/derivatives, phenylpropanoids (C<sub>6</sub>-C<sub>3</sub>), and shikimates/phenylpropanoids are potential biosynthetic routes for this query metabolite, supporting the obtained results (Fig. 3).

## Taxifolin

Structural annotation correctness also improved for the negative parent ion at  $m/z$  303.0502, which ranked taxifolin as the best match (1st) among hundreds of structures from Biodatabases (Fig. 4). Molecular fingerprint detection clearly showed an existing of basic flavonol ring system, characterized by C6(ring A)-C3(ring C)-C6(ring B), in this query subject. Substructures encode by “C(C(Coc:1:c:c(:c: c:2)~[#8])~[#8])c:1:2” (ring A), “CCC(=O)c1cccc1” (ring B), “ECFP6: 1580559118” (relationship between rings C and B), and “[#6]~C(c(:c:c(:c:1)~[#11]): c1)~[#11]” (ring B)” illustrate the atomic correlation between rings A, C, and B within the taxifolin structure. The MS/MS spectrum closely matches those in PubChem <https://pubchem.ncbi.nlm.nih.gov/image/ms.cgi?peaks=273.041:999,125.024:583,255.03:284,301.036:238,227.036:212>), especially the base peak at  $m/z$  125.0252, indicating a common fragmentation pathway. Dihydroflavonols, flavonoids, and shikimate/phenylpropanoid pathways were predicted as its natural product classes, supporting the biosynthetic origins of this natural product.

*Luteolin 7-glucuronide*

A similar predicted pattern was observed with the positive precursor ion ( $m/z$  463.0890), which was identified as luteolin 7-glucuronide (1st) by both SIRIUS and the MetFrag. In this instance, fingerprints indicating the

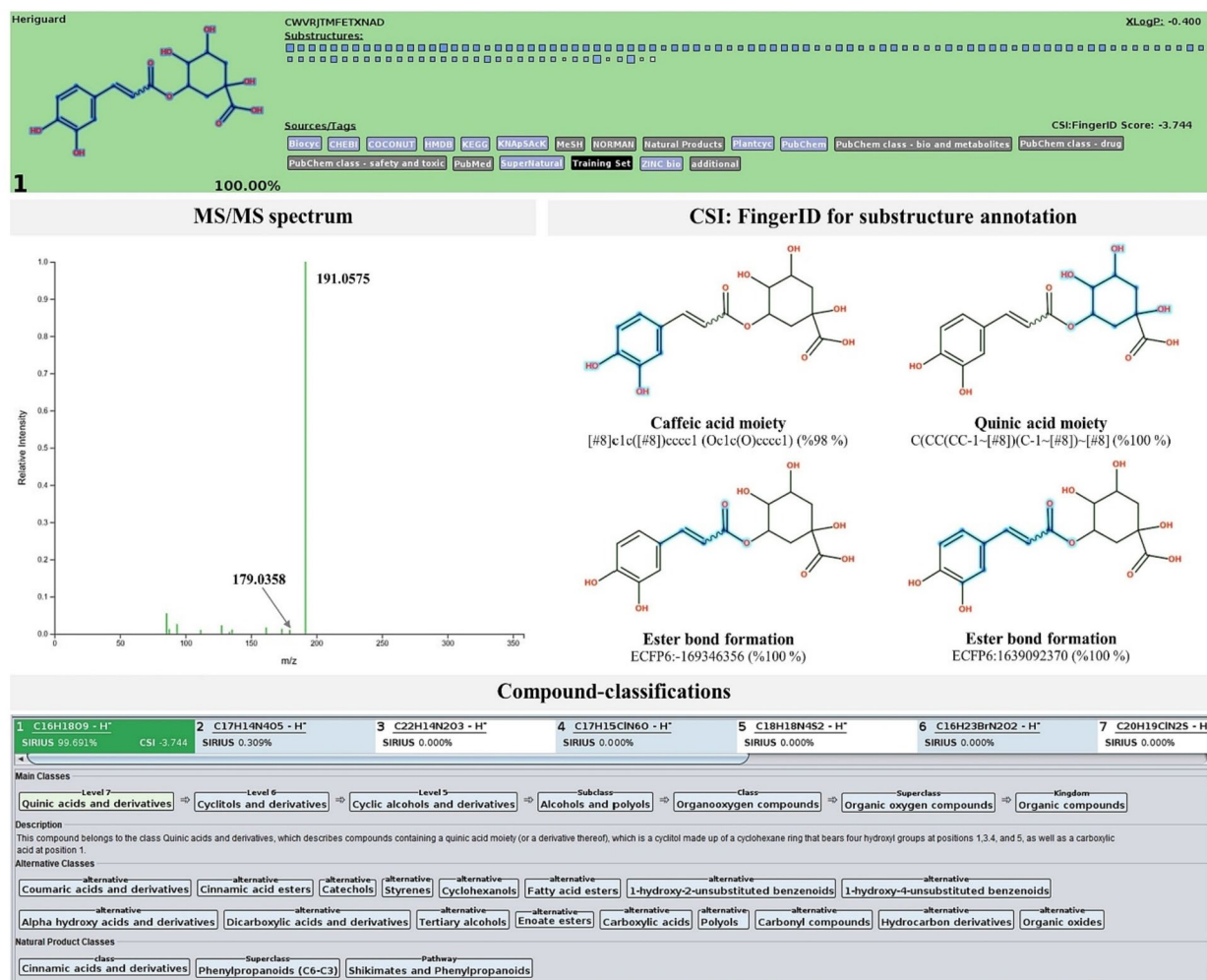


**Fig. 3.** Structural annotation of putative chlorogenic acid.

attachment of the glucuronide moiety to the aglycone core structure such as “CC(O)C(O)C(O)C(O)CO (glucuronide moiety)”, “OCC(=O)O (glucuronide)”, “[#6] ~ O[CH1]([CH1]([CH1]([CH1]([CH391]1[CH0]. (~[OH1D1])~[OH1D1])~O)~O)[OH0]1 (glucuronide)”, and “c(:c(:c(:c(:c1~[#8])~[#8]): c1~[#] (ring A attached to glucuronide unit)” were clearly detected (Fig. 5). The emergence of the fragment ion with  $m/z$  287.0578 (base peak) signifies the complete loss of the glucuronide from the luteolin moiety. This is highly similar to the MS/MS spectrum of authentic luteolin 7-glucuronide from PubChem (<https://pubchem.ncbi.nlm.nih.gov/compound/Luteolin-7-glucuronide#section=Spectral-Information>), suggesting they were the same substance.

#### Germacrone

Germacrone ( $m/z$  219.1393) was also supposed to occur in the *C. mimosoides* aqueous ethanolic extract. Despite a greater mass error deviation (−162.43 ppm) and not achieving a top rank in MetFrag (7th; KEGG), narrowing the search to appropriate databases increases the reliability of predicting this natural product. According to the CSI: FingerID, the cyclic sesquiterpene (C<sub>15</sub>H<sub>22</sub>O; SIRSUS score 100%) was the top-ranked candidate in the ZINC, MeSH, and PubMed databases, possibly due to its existence in the structural training set (<https://www.cs-fingerid.uni-jena.de/>).

v3.0/api/fingerid/trainingstructures? predictor=1). Molecular fingerprints illustrating the successive cyclization of three C5 isoprene units to form a C15 sesquiterpene were deduced with high posterior probability scores, such as ‘CCC=C(C)C (83%)’, ‘CC(=O)C (79%)’, and ‘[#6]=#6~[#6] (90%)’. Sesquiterpenoids and terpenoids are predicted to be the principal natural product classes, thereby supporting the biosynthetic origins of this query subject (Fig. 6).

#### Anti-viral and hemolytic activities of the plant extracts

Cytotoxicity assays against MDCK cells were conducted, revealing a cytotoxicity concentration (CC<sub>50</sub>) of greater than 50 µg/mL and identifying a range of extract concentrations found to be non-toxic. After diluting within the non-toxic range, the extracts were immediately pre-mixed with the virus before



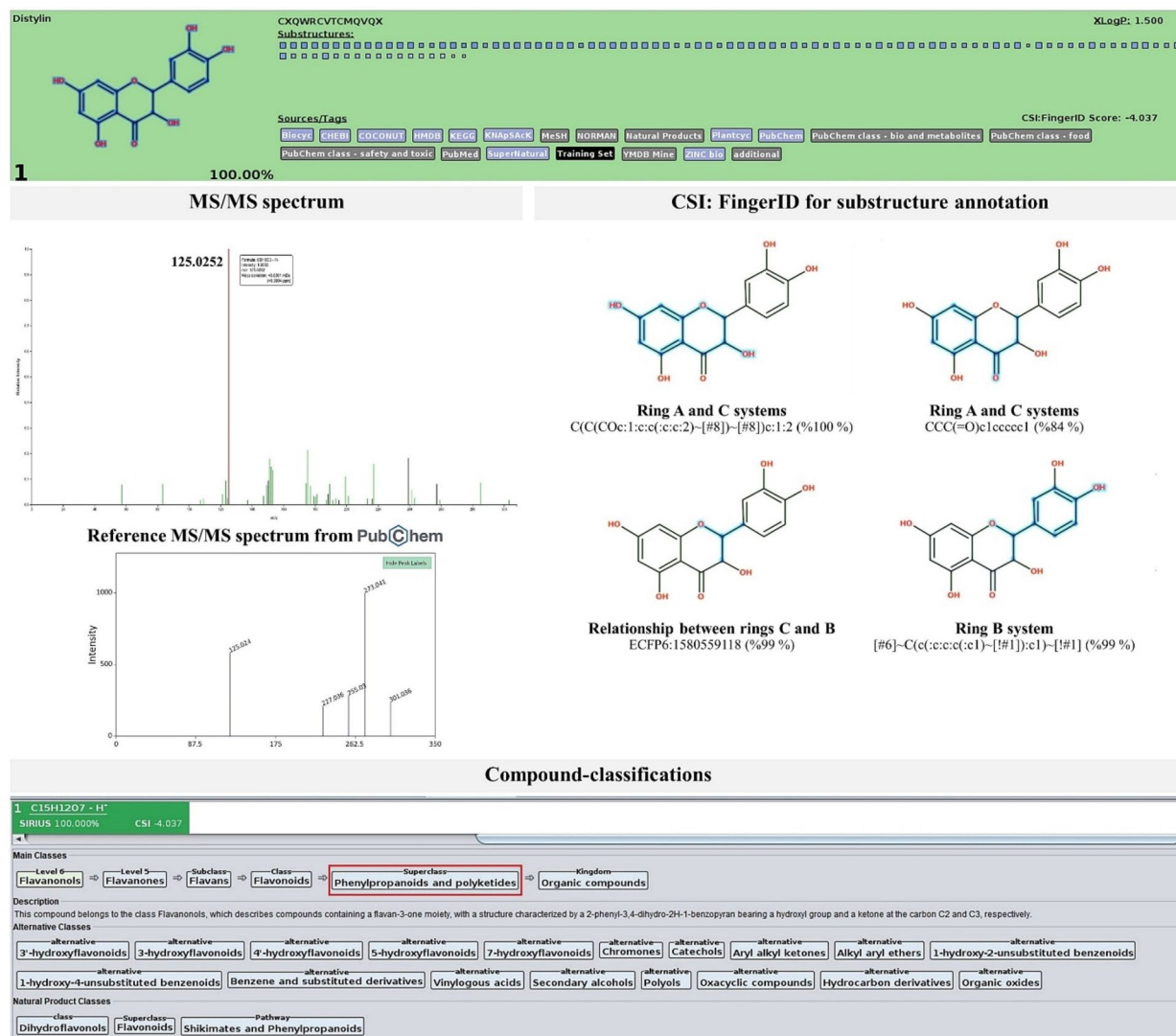


**Fig. 4.** Structural annotation of putative Taxifolin.

being added to MDCK cells for infection. The mixture was incubated with the cells for 24 h, allowing for the antiviral assessment throughout the viral life cycle. The *C. mimosoides* hydroethanolic extract demonstrated an  $IC_{50}$  of 2.33  $\mu\text{g/mL}$ , showing approximately 3.35-fold and 1.96-fold higher potency compared to the controls—the aqueous extract and gallic acid, respectively (Fig. 7; Table 4). This result might indicate that the increase in gallic acid content in the plant extracts did not correlate with enhanced antiviral activity, and that other phytochemicals may provide a synergistic effect in this phenomenon. Since the plant extract was present from the attachment through the replication and budding stages, its inhibitory effect may arise at various stages of the viral life cycle. The significant difference between  $IC_{50}$  and  $CC_{50}$  values also demonstrates the extract's effectiveness without detrimental effects on MDCK cells. It remarkably did not show hemolytic activity towards hRBCs, even at the highest concentration tested (2000  $\mu\text{g/mL}$ ). Therefore, the hydroethanolic plant extract could be a safe and effective antiviral solution (Table 4).

### Target specificity of chosen metabolites against the H1N1 proteins

Molecular docking was then carried out to explain mechanisms of actions underlying anti influenza activity of the *C. mimosoides* aqueous ethanolic extract. Since the plant extract was exposed to multiple stages of the viral life cycle (e.g., attachment, entry, replication, and release), HA, NA, and PB2 have been chosen as promising targets in this study. Meanwhile, many flavonoids (e.g., quercetin, isorhamnetin, rutin, and quercetin 7-O-glucoside) have been demonstrated to show multiple inhibitory effects with the aforementioned proteins<sup>35,40,41</sup>. While specific inhibition of other subunits of influenza RNA polymerase (e.g., PA, NP) remains unclear, Gansukh and colleagues demonstrated that quercetin derivatives strongly interact with PB2, resulting in decreased expression of genes encoding M2 and NP, suggesting that PB2 is a probable target in addition to NA<sup>42</sup>. This finding appears to correlate with in silico studies showing that quercetin interacts with NA at a higher binding energy

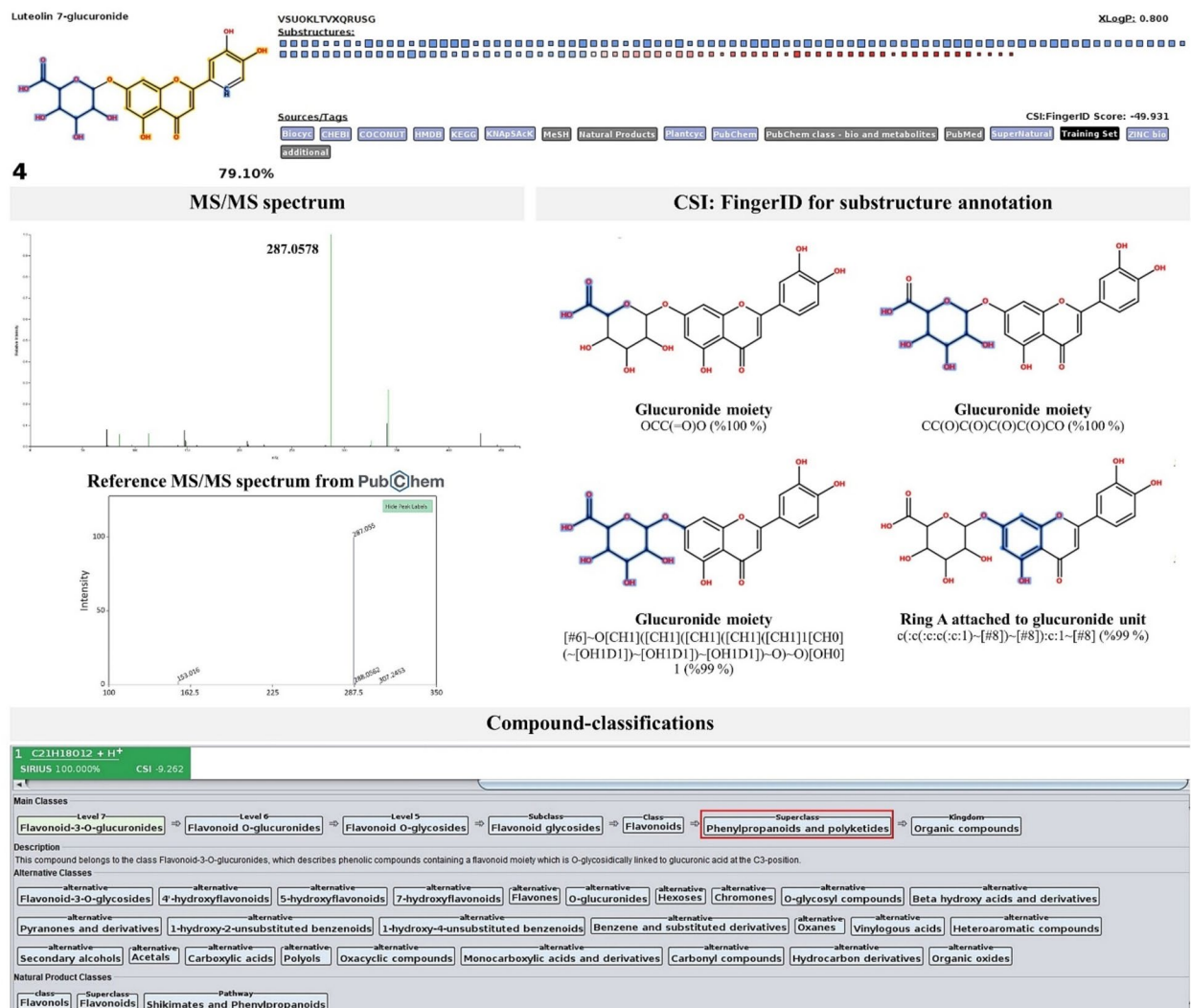


**Fig. 5.** Structural annotation of putative luteolin 7-glucuronide.

(−6.8 kcal/mol) compared to its interaction with the M2 protein (−5.48 kcal/mol)<sup>29</sup>. Hence, it may be possible to consider M2 as an unlikely target based on our findings. Molecular docking studies revealed that all docked metabolites preferentially interacted with NA and PB2, as indicated by the minimal differences in fitness scores (GOLD score). A high fitness score predicts the ligand binding position with strong binding affinity between two molecules, calculated based on chemical binding energies, including hydrogen bonding, van der Waals forces, metal interactions, and ligand torsional strain<sup>43</sup>. Comparing the three chosen target-specific proteins, the fitness scores (Gold scores) calculated via the GOLD program for quercetin interacting with NA and PB2 (57.29 and 59.86, respectively) are higher than that for HA (47.66) (Table 5). This result may suggest that the HA-ligand complex has a lower binding affinity compared to the interactions of NA and PB2 with the same metabolite. Therefore, HA might serve as an off-target inhibitor in our case. Notably, since gallic acid, catechin, quercetin, chlorogenic acid, their glycoside derivatives (e.g., quercetin-7-O-glucoside), and polyphenol-rich extracts (PRE) can reduce HA mRNA transcription and NP protein synthesis in a dose-dependent manner in IAV-infected cells<sup>8,40,41,44</sup>, this inhibitory effect may potentially arise from interference with the influenza RNA polymerase complex—composed of PA, PB1, and PB2—rather than from direct inhibition of HA and NP proteins, due to its regulatory role in controlling the transcription of the machinery proteins<sup>29</sup>. While specific inhibition of shikimate- and phenylpropanoid-derived natural products against various subunits of the RNA-dependent RNA polymerase (RdRp) of influenza A remains limited, recent in silico studies indicate that quercetin derivatives exhibit high binding activity at the cap-binding site of the PB2 subunit, comparable to favipiravir and mGTP<sup>42</sup>. All the above considerations lead us to suggest that NA and PB2 are more likely targets of the identified metabolites found in the *C. mimosoides* hydroethanolic extract than HA and even M2 coding proteins. Although shikimic acid, pyrogallol, and quinic acid—among the top five most abundant phenolics in the hydroethanolic extract—showed limited interaction with the two target proteins (compared with gallic acid), they may still play a protective role by neutralizing oxygen radicals produced during viral infection due to their antioxidant activities<sup>45</sup>.

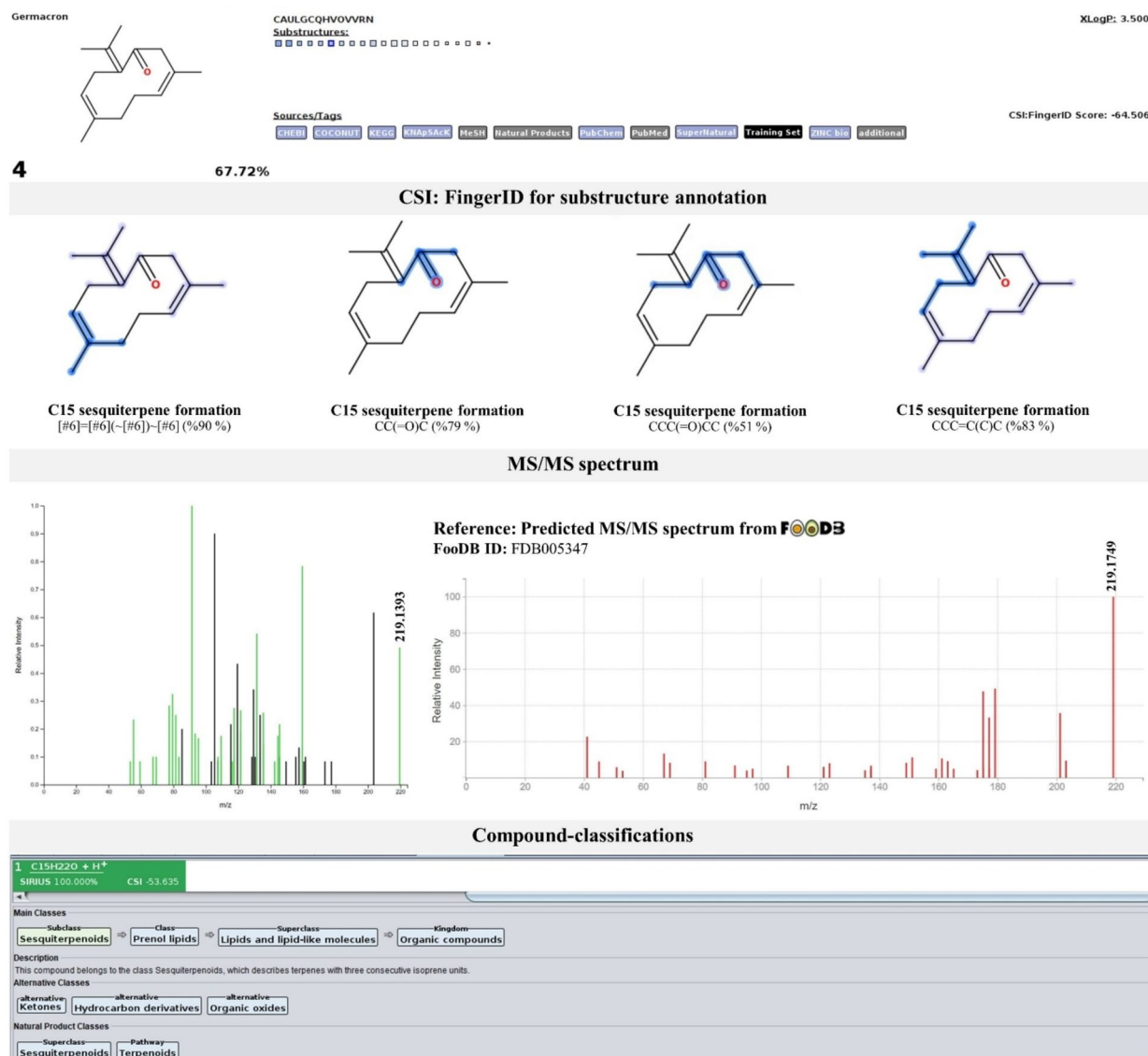


**Fig. 6.** Structural annotation of putative mass peak germacrone that is resembled to those simulated in database ([https://foodb.ca/spectra/ms\\_ms/74446#spectrum](https://foodb.ca/spectra/ms_ms/74446#spectrum)).

### Molecular docking against neuraminidase (NA)

As outlined in recent literature, gallic acid and its two alkylated derivatives, methyl gallate and ethyl gallate, which were isolated from the aqueous extract of *Radix paeoniae* Alba, show potential as neuraminidase inhibitors although they are slightly less potent than oseltamivir acid<sup>36</sup>. The binding affinity of gallic acid and its methylated analogs will determine the inhibitory effects of other phytochemical constituents. Any compounds with a predicted fitness score higher or slightly different from 46.75 will be considered to have biological activity. They should also specifically interact with the catalytic residues by forming conventional hydrogen and/or electrostatic bonds, with bond distances not exceeding 3.00 and 5.00 Å, respectively<sup>46</sup>. Meeting these criteria, 26 out of 35 docked metabolites were suggested to have anti-influenza activities, and their details are provided below.

### Simple phenolic and flavonoid derivatives

Previous research has demonstrated the potent anti-influenza activity of shikimate and phenylpropanoid-derived natural products, which can bind strongly to the active site of neuraminidase (NA) and inhibit viral growth cycles more effectively than conventional neuraminidase inhibitors, such as oseltamivir and zanamivir<sup>32,47,48</sup>. In our study, the phenolics found in the hydroethanolic extract of *C. mimosoides*, specifically flavonoids and glycosylated derivatives, displayed promising binding affinities towards NA structure, comparable to the referent drug, oseltamivir-1-carboxylic acid, and they share the same binding region. Guaijaverin, the most potent phenolic, interacted with ten critical residues including Arg118, Glu119, Ile149, Lys150, Arg152, Arg278, Arg293, and Arg368 in the inner shell of NA structure through H-bond (1.69–2.93 Å),  $\pi$ -lone pair, and  $\pi$ -cation

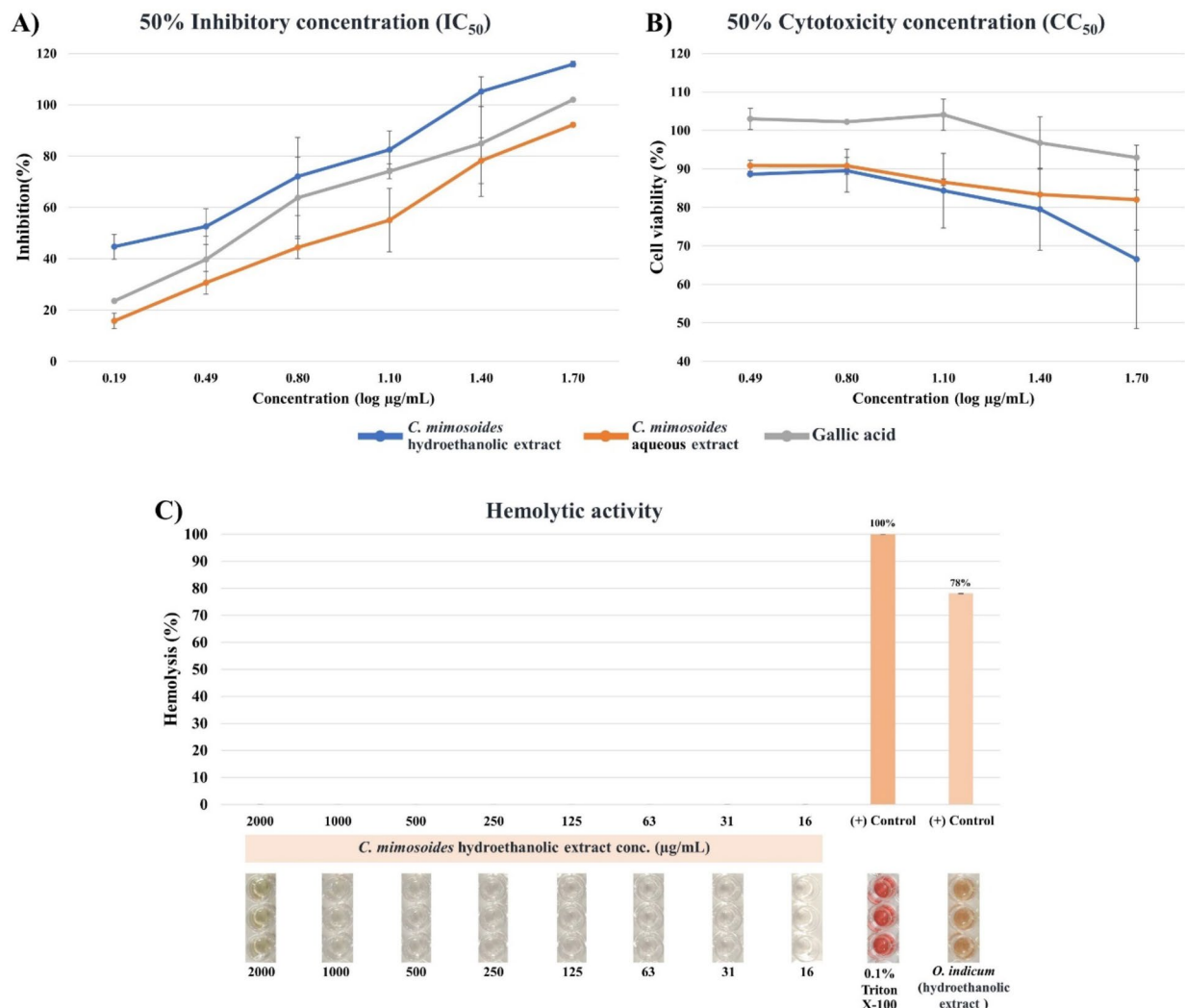


**Fig. 7.** Antiviral activity of the *C. mimosoides* extract. Lower IC<sub>50</sub> values indicate greater antiviral potency. CC<sub>50</sub> is defined as the concentration needed to reduce MDCK cell viability by 50%. The extract's IC<sub>50</sub> is much lower than its CC<sub>50</sub>, demonstrating effective antiviral action without harming host cells. Triton-X (0.1% v/v) and hydroethanolic extract of *Oroxylum indicum* were positive controls in this study.

Sample	Anti-influenza A/Puerto Rico/8/34 (H1N1)			Hemolytic activity (µg/mL)
	IC <sub>50</sub> (µg/mL)	Gallic acid content (µg/mL)	CC <sub>50</sub> (µg/mL)	
Hydroethanolic extract (30% v/v)	2.33	0.87	> 50	> 2000
Aqueous extract	7.81	4.20	> 50	> 800
Gallic acid	4.56	–	> 100	N.A.

**Table 4.** Comparison of anti-influenza and hemolytic activities of *C. mimosoides*.

interactions with Thr438 (2.69 Å), Ile149 (2.57 Å), and Arg156 (3.15 Å), respectively (Fig. 8). Additionally, quercetin 7-O-glucoside exhibited comparable binding characteristics to guaijaverin by forming four H-bonds with Asp151, Glu277, Arg293, and Arg368, and engaging in  $\pi$ -cation,  $\pi$ -alkyl, and  $\pi$ -donor H-bonds with Arg118, Lys150, and Tyr402, playing a crucial role in binding with sialic acid and oseltamivir<sup>49</sup>. Two glycosylated kaempferol derivatives, astragalin and afzelin, displayed even more potent binding affinities than the two positive referent ligands, oseltamivir carboxylic acid. Astragalin interacted with six critical residues (Arg118, Ile149, Asp151, and Arg152) using its glucose moiety and C ring system (2.14–2.91 Å) and formed various hydrophobic interactions with Lys150 (3.10 Å), Glu278 (4.56–4.78 Å), Arg293 (4.02–4.36 Å), and Tyr402 (5.96 Å), respectively. Afzelin interacted with the highly conserved residues (Glu119, Trp179, Ser180, Lys150, Arg293,

Compound		Fitness score (Gold score)		
		NA (PDB: 6HP0)	HA (PDB: 1RU7)	PB2 (PDB: 4NCE)
<i>C. mimosoides</i> 's metabolites				
1	4-Hydroxybenzoic acid	35.18	28.35	40.92
2	Gallic acid	46.75	33.50	42.26
3	Malonic acid	33.49	21.71	25.58
4	Inositol	40.70	28.69	34.01
5	Pyrogallol	43.75	31.17	37.46
6	Azelaic acid	51.36	37.40	44.46
7	Trigonelline	48.91	31.03	39.95
8	Quinic acid	41.69	32.71	36.84
9	6-Methylcoumarin	43.62	29.45	44.29
10	Shikimic acid	41.72	32.34	41.79
11	Hexadecanedioic acid	64.22	46.43	58.67
12	Tetradecanedioic acid	60.22	41.37	59.00
13	Ethyl gallate	54.62	38.32	51.26
14	Undecanedioic acid	57.18	39.94	49.93
15	Gallocatechin	66.66	42.60	60.04
16	2,6-Dihydroxy-4-methylbenzoic acid	45.15	33.82	45.21
17	(-)-Catechin	55.88	45.28	58.97
18	Dihydromyricetin	61.85	44.22	60.77
19	D-Pinitol	42.11	30.13	36.43
20	Scutellarin	72.59	61.94	73.69
21	Quercetin*	57.29	47.66	59.86
22	Quercitrin	69.38	54.90	69.54
23	Luteolin 7-glucuronide	71.74	60.12	73.87
24	Esculetin	42.46	35.26	48.09
25	Myricetin	62.44	46.90	60.99
26	Myricitrin	72.47	56.60	69.98
27	Ellagic acid	58.73	45.68	63.87
28	Astragalin	69.51	49.30	69.42
29	Afzelin	68.83	53.40	69.08
30	(E)-beta-Damascone	42.74	31.14	42.81
31	Guaijaverin	77.08	52.36	68.21
32	Germacrone	43.55	29.29	41.13
33	4-coumaric acid	39.75	32.73	44.47
34	Taxifolin	58.23	44.41	–
35	Chlorogenic acid	59.54	40.87	59.60
Reference ligands				
36	Isoquercetin	73.46	51.60	70.99
37	Rutin	79.53	51.62	–
38	Hyperoside	80.57	51.95	–
39	Isorhamnetin	59.62	48.69	61.22
40	Quercetin 7-O-glucoside	74.68	51.50	69.09
41	Oseltamivir carboxylic acid	61.55	43.48	–
42	GJT	90.51	–	–
43	O-sialic acid	–	48.72	–
44	mGTP	–	–	109.42
45	Favipiravir-RTP	–	–	82.03

**Table 5.** Target specificity of query metabolites towards HA, NA, and PB2-subunit of influenza A/PR/8/34 virus.

and Arg368) through ten H-bonds and formed  $\pi$ -cation,  $\pi$ - $\pi$ -T-shaped, and  $\pi$ -alkyl interactions through its flavonol basic ring system. Since gallic acid, quercetin, rhamnetin, and isorhamnetin have also been found to possess anti-influenza properties by exhibiting significant binding capabilities to NA from H1N1 (A/PR/8/34), similar to the drug zanamivir<sup>36,42</sup>, the same inhibitory effects of other flavonoids, including myricetin, myricitrin, dihydromyricetin, quercitrin, scutellarin, and luteolin 7-glucuronide, are highly promising. Upon closer



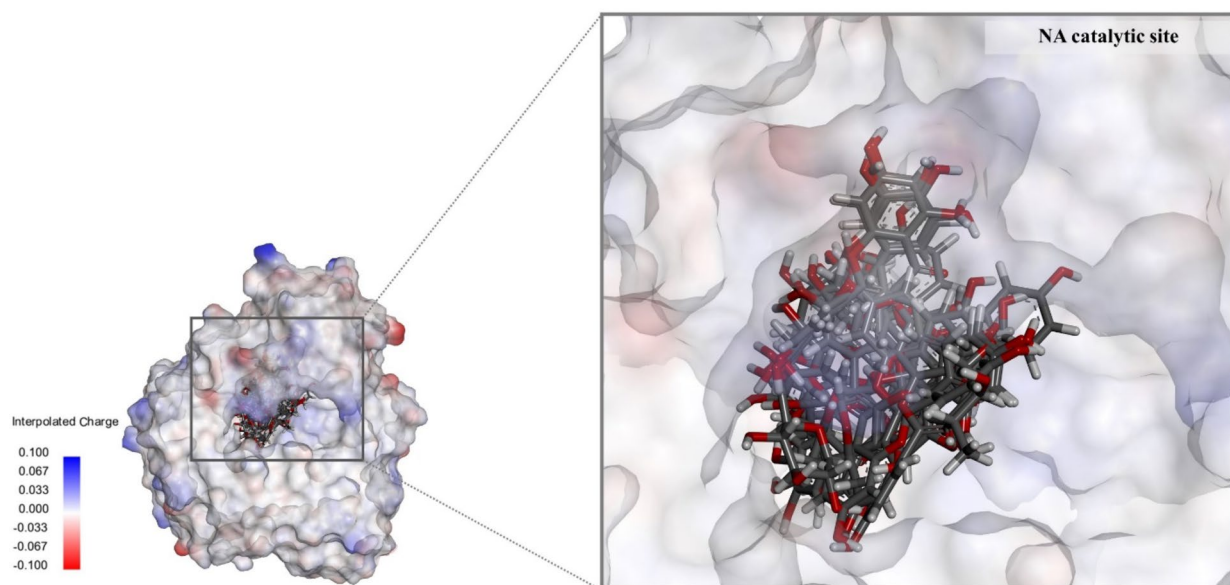


**Fig. 8.** Ligand – receptor interaction of chosen polyphenols with the catalytic residues of NA structure.

examination, they exhibited strong interactions against the key amino acid residues, resulting in remarkable binding values ranging from 61.85 to 72.59. For instance, luteolin 7-glucuronide forms five hydrogen bonds with active amino acids, including Asp151, Arg152, Trp179, Arg293, and Arg368, utilizing its free carboxyl and hydroxyl groups. Its aromatic core structure also engaged in numerous hydrophobic interactions with Arg118, Ile149, Asp151, and Tyr402. In light of our observations, glycosylated flavonoids generally exhibit stronger binding properties than their parent compounds in biosynthetic pathways. For instance, myricitrin demonstrated superior binding compared to myricitrin and dihydromyricitrin presumably due to the existence of a rhamnopyranosyl moiety that enables the creation of three exclusive H-bonds with Arg368 and Arg293, not existing in its parent structures. Mothlhatlego et al.<sup>50</sup> demonstrated that myricetin 3-O-rhamnoside, isolated from *Newtonia buchananii*, inhibits various stages of the influenza A life cycle, including attachment and entry, suggesting NA as a promising antiviral target here. It could also be reinforced by a recent study indicating the synergistic effects of multiple flavonoids—myricetin, quercetin, quercitrin, amentoflavone, and afzelin—found in *Thuja orientalis* folium extract, leading to substantial inhibition of influenza A virus (A/PR/8/34) attachment and entry, mediated by the inhibition of NA activity<sup>46</sup>. Similar reasons may be relevant for (-)-catechin and gallic acid, where the latter created nine H-bonds with the putative catalytic inner residues, a higher number compared to (-)-catechin, which formed five H-bonds in the expected region. We also observed their proximity to oseltamivir acid binding site, suggesting their potential to inhibit the enzyme activity (Fig. 9). The article reviewed by Ide et al.<sup>51,52</sup> also shows that various catechins (e.g., EGCG, epicatechin gallate, and catechin-5-gallate) exhibit anti-influenza virus effects by interacting differently with the neuraminidase structure, as proposed in molecular docking studies. Our findings imply that the binding efficiency of various flavonoids found in the *C. mimosoides* hydroethanolic extract depends on the number and strength of interactions with the target region, thus highlighting polyphenol-rich extracts as natural anti-neuraminidase agents<sup>53</sup>.

Concerning simple phenolics (Fig. 10), chlorogenic acid can reveal six H-bonds with the important residues, Thr148, Glu119, Arg152, Trp179, Glu278, and Tyr402, where hydrophobic interactions and C-H bonds were formed by the residues Arg156, Thr148, and Gly147. Ding et al. (2017) provided clear evidence supporting our assumption, showing that chlorogenic acid acts as a neuraminidase blocker, effectively inhibiting influenza A virus in both in vitro and in vivo models<sup>54</sup>. A recent study also indicated that the higher levels of chlorogenic acid in decaffeinated coffee beans, combined with lower caffeine levels, significantly impact their ability to inhibit neuraminidase<sup>55</sup>. Despite gallic acid, ethyl gallate, and ellagic acid displaying lower fitness score compared to oseltamivir carboxylic acid (the referent ligand), they should still be recognized as bioactive due to their ability to interact with NA catalytic residues, supported by previous in vitro testing models<sup>56</sup>. In doing this, gallic acid formed six promising H-bonds with Arg118, Glu119, Arg293, and Arg368 (2.02–2.65 Å) using its three hydroxyl groups. Moreover, its  $\pi$ -system localizing in benzene ring facilitated hydrophobic bonds with Arg293 (3.86 Å), Lys150 (3.72 Å), Glu278 (3.66 Å), and Tyr402 (2.46 Å) located around the central ligand. A comparable trend was observed with ethyl gallate, except it likewise formed C-H bonds with Glu227 due to the ethoxy group, gaining a higher binding energy than its chemical ancestor. Ellagic acid generated five H-bonds with active residues, including Arg118, Glu227, Glu228, Arg293, and Arg368. Its dimeric ring system efficiently created numerous  $\pi$ -interactions with Lys150, Arg225, Glu278, and Tyr402 (Fig. 10B). Also, it was found that gallic acid, ethyl gallate, and ellagic acid are oriented near oseltamivir acid, implying they have the potential to inhibit the neuraminidase enzyme (Fig. 10A). Our results resemble to findings that ellagic acid, one of the four major polyphenols present in *Punica granatum* extract (PPE), individually exhibits anti-influenza activity and shows a synergistic effect when combined with oseltamivir<sup>57</sup>.

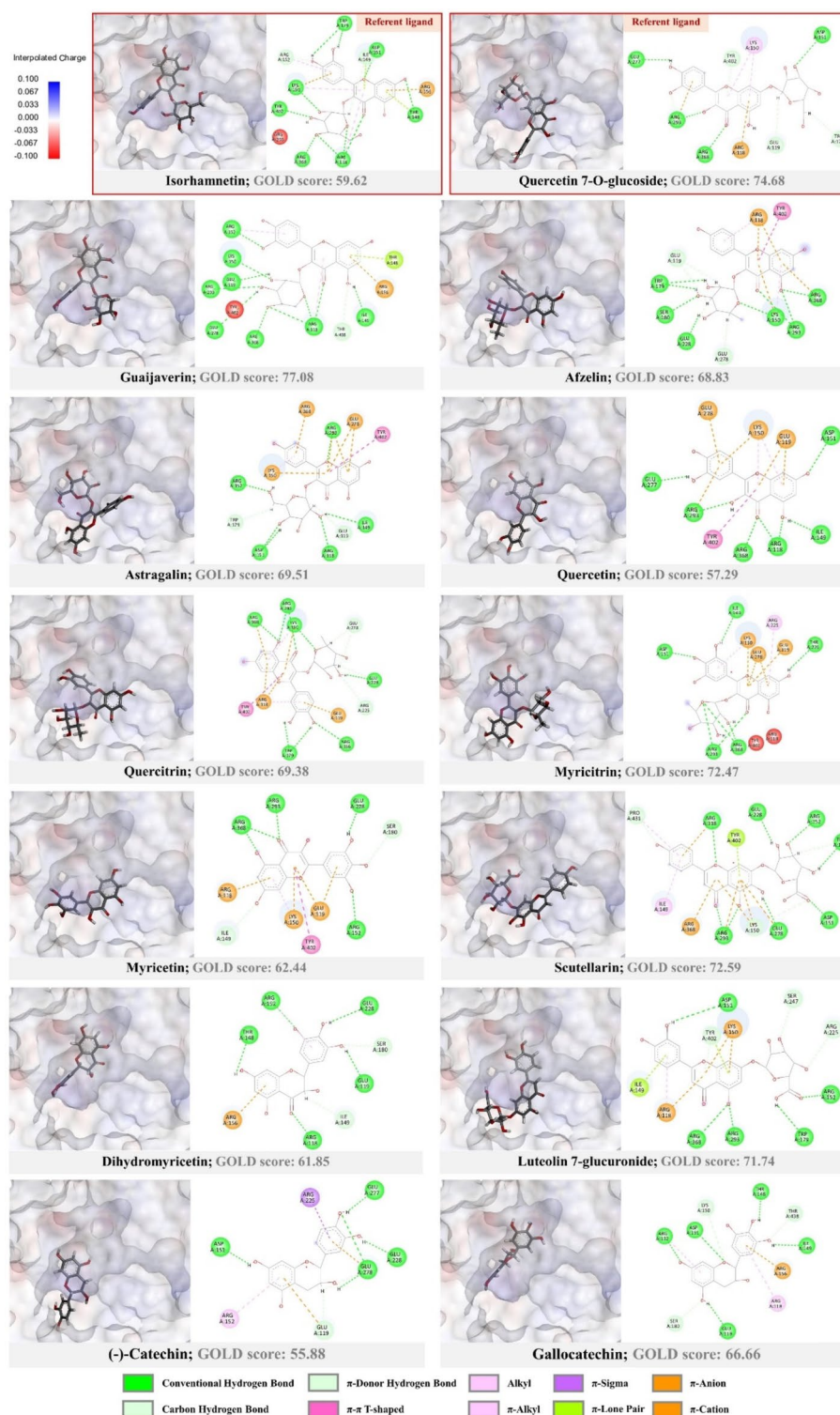


**Fig. 9.** Structural orientation of flavonoids and glycoside derivatives within the oseltamivir recognition site in NA structure (PDB: 6HP0).

### Non-polyphenols against NA

Studies have found that phenolic and non-phenolic substances inhibit the viral cycles synergistically, although they might have limited antiviral properties independently. It is, therefore, essential to investigate compound interactions for potential therapeutic implications. Herein, various non-polyphenols, including dicarboxylic acids (e.g., hexa-, tetra-, and undecane-dioic acids), terpenoids (germacrone), and alkaloids (trigonelline) were simultaneously detected in the hydroethanolic *C. mimosoides* extract. They were all found to have comparable or

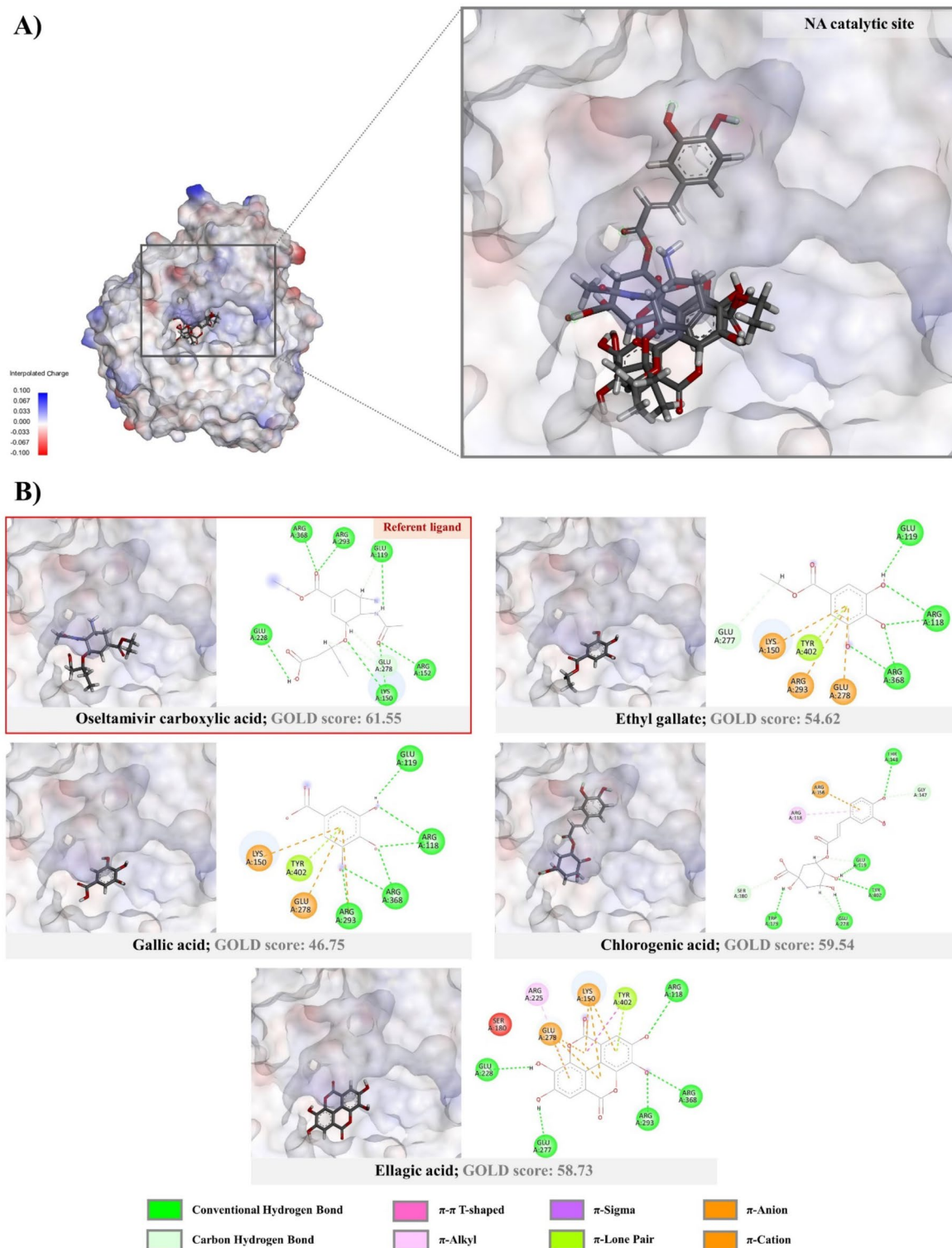


**Fig. 10.** (A) Structural orientation of simple phenolics located in the active site of NA structure. (B) 2D and 3D structures that illustrating their binding potential with the drug recognition site.

remarkably higher fitness scores equated with the reference ligands, e.g., gallic acid, quercetin, and rhamnetin) (Table 5; Fig. 11). Considering dicarboxylic acids, with fitness scores range from 51.36 to 64.22, occupy with the highly conserved residues of NA structure through both H-bonding and alkyl interactions, maintaining distances within the proper ranges. Hexadecanedioic acid, for example, formed three H-bonds with Lys150, Arg156, and Arg156 together with three alkyl-alkyl interactions with arginine triad (118, 152, and 225) (Fig. 11B). Similarly, tetradecanedioic acid whose fitness score is 60.22, reveals three H-bonds (Lys150, Arg156, and Glu278)



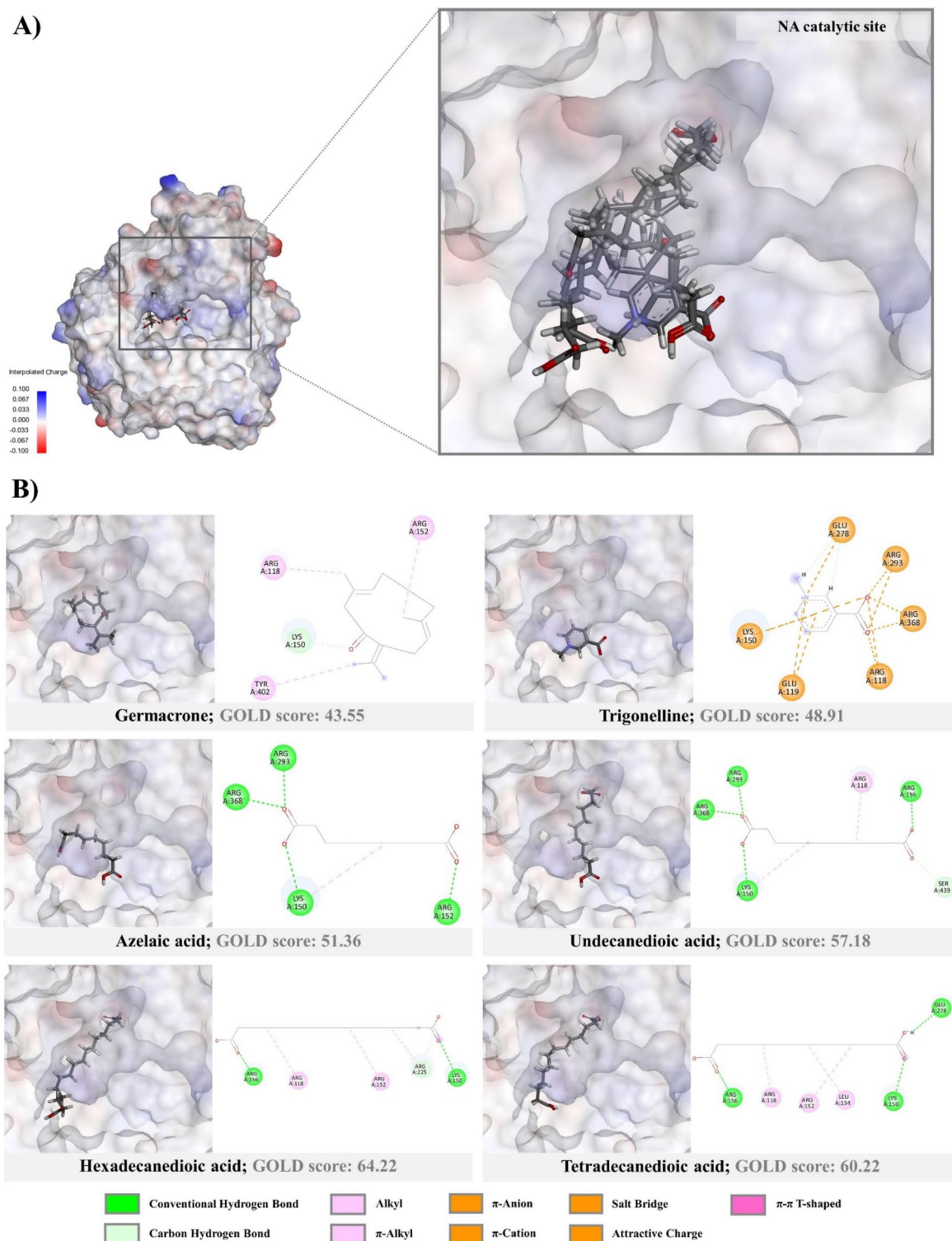


**Fig. 11.** (A) Non-phenolic substances are predicted to orient within NA catalytic site. (B) Their specific interactions with the drug/sialic acid recognition pocket.

together with forming alkyl bonds with those lining catalytic inner shells, including Arg118, Leu134, and Arg152. Azelaic acid and undecanedioic acid, the shorter chain fatty acids, forming four H-bonds with Arg152, Arg156, Arg293, Arg368, and Lys150, where they also used the alkyl systems generating alkyl interactions with Lys150 and Arg118, hence receiving the higher binding scores over specific referent ligand (e.g., gallic acid). These results also indicated their binding affinities diminished in the following order: Hexadecanedioic acid > tetradecanedioic acid > undecanedioic acid > azelaic acid, significantly correlated with the number of

carbon atoms and interactions between the ligand and target protein (NA). Trigonelline, an alkaloid, could form two C-H bonds with Glu228 while establishing multiple attractive charges with NA inner shell. Germacrone, with binding energy almost identical to gallic acid, formed C-H,  $\pi$ -alkyl, and alkyl interactions with Lys150, Arg118, and Arg152, maintaining appropriate distances ( $\leq 3.00$  Å for H-bonds,  $\leq 5.00$  Å for hydrophobic interactions) and shared the binding pocket with selected neuraminidase inhibitors, as revealed by binding orientation analysis (Fig. 11A). This evidence is supported by Liao et al.<sup>58</sup>, showing that germacrone, derived from *Rhizoma curcuma* essential oil, inhibits the influenza life cycle's early stages and replication processes.

### Molecular docking of against cap-binding domain (PB2)

A significant number of phenylpropanoid-derived natural products have been identified as effective inhibitors of influenza virus replication, in addition to their role as neuraminidase blockers<sup>59</sup>. By mimicking the binding properties of mGTP and Favipiravir-RTP (reference ligands), they achieve this by forming various hydrophobic interactions (e.g., alkyl,  $\pi$ - $\pi$  T-shaped,  $\pi$ - $\pi$  stacked) with highly conserved amino acid residues (such as Phe323, His357, Phe363, and Phe404) within the cap-binding domain, thereby disrupting the viral cycle<sup>60</sup>. Besides exhibiting the probability to penetrate the viral envelope<sup>61</sup>, characterized by logP values ranging from 0.21 to 1.8 (Table 3), the target specificity assay revealed that a variety of simple phenolics and flavonoids exhibit strong interaction with PB2 subunit, with comparable scores to those observed with neuraminidase (Table 5). You et al.<sup>8</sup> reported that gallic acid from *Toona sinensis* leaf extract also showed polypharmacological effects, inhibiting influenza virus replication with IC<sub>50</sub> and CC<sub>50</sub> values of 18.14 and  $>100$  µg/mL, respectively. Therefore, compounds scoring close to or above 42.71 are likely active and expected to interact with the cap-binding domain. This involves forming a range of H-bonds and hydrophobic interactions, with bond distances not exceeding 3.00 Å and 5.00 Å, respectively<sup>46</sup>. Based on these criteria, 27 metabolites were selected to explain the potential mechanisms underlying anti-influenza activity, as detailed below.

#### Simple phenolic compounds against cap-binding protein (PB2)

Twenty polyphenols were identified as capable of interacting with the crucial hydrophobic residues within the cap-binding domain of PB2 subunit, displaying a binding orientation highly resembling those of mGTP, favipiravir-RTP, and quercetin (Fig. 12). They importantly engaged in  $\pi$ -stacking interactions with Phe363 and Phe404, crucial for cap-binding by influenza RNA polymerases<sup>53</sup>, and could interact with nearby aromatic amino acids, thus resulting in enhanced complex stabilization. To begin with, consider the simple phenolics (gallic acid, ethyl gallate, *p*-coumaric acid, ellagic acid, and chlorogenic acid) with binding scores ranging from 42.26 to 63.87 (Table 5). Gallic acid, the second most abundant phenolic detected in hydroethanolic extract, created three  $\pi$ - $\pi$  stacked interactions with Phe323 (5.32 Å), His357 (4.02 Å), and Phe404 (3.70 Å) while forming strong H-bonds with Glu361, Lys376, and Phe404 (1.95–2.16 Å) (Fig. 12B). Notably, a significant number of hydrophobic interactions are observed in its more lipophilic derivatives—ethyl gallate and ellagic acid, with logP values of 1.21 and 0.79, respectively. The former exhibited multiple types of  $\pi$ -interactions with His357 (3.49–5.04 Å), Phe323 (2.66–4.34 Å), and Phe363 (5.47 Å) while establishing multiple H-bonds with Ser337 (2.86 Å), Glu361 (1.83 Å), Lys376 (2.73 Å), and Phe404 (2.37 Å), effectively anchoring in the sialic acid/drug binding pose. These results align with previous studies, showing that extracts from *Radix paeoniae Alba* and *Punica granatum*, rich in gallic acid and its alkyl derivatives, inhibit influenza A virus replication in MDCK cells<sup>36</sup>. The latter, a dimeric form of gallic acid, generated thirteen crucial hydrophobic interactions with Phe323, Phe325, Phe357, Phe363, and Phe404, due to the increased number of  $\pi$ -systems, along with three hydrogen bonds with Ser337 (3.05 Å) and Glu361 (2.05 and 2.08 Å). This elaborated the existing finding that *Aronia melanocarpa* extract, rich in ellagic acid and myricetin, shows antiviral activity against influenza viruses and protects mice from lethal influenza challenges<sup>10</sup>. 4-Coumaric acid capable of interacting with His357 and Phe404 via two  $\pi$ - $\pi$ -stacked interactions (4.0 and 3.73 Å), coexisting with two rigid H-bonds with Phe404 and Arg332 (1.56–2.64 Å). As found in the literature, 4-coumaric acid, a key component of Brazilian propolis (AF-08), demonstrated anti-influenza activity (A/PR/8/34(H1N1), with IC<sub>50</sub> and CC<sub>50</sub> values of  $31.5 \pm 1.3$  µg/mL and  $>100$  µg/mL, respectively, highlighting its potential antiviral properties<sup>56</sup>. Although chlorogenic acid is known as a neuraminidase blocker, its multiple effects on the cap-binding domain should be explored due to its fitness score (59.60) and moderate hydrophobicity. This compound established three promising  $\pi$ - $\pi$  stacked interactions with His357, Phe404, and Phe323 (3.78–5.74 Å), along with multiple H-bonds with Arg332, Ser337, Lys339, His367, and Phe404 (1.59–2.93 Å), resembling the molecular recognition and interaction of mGTP and favipiravir-RTP (Fig. 12A). While direct evidence to support our supposition remains unclear, a computational study conducted by Luo et al.<sup>62</sup> showed that chlorogenic acid, one of the major phenolic substances in *Lonicera japonica*, exerts a synergistic effect against both NA and PB2, which are crucial for the influenza life cycle, shedding light on the multiple effects of natural products reported herein.

#### Flavonoids against cap-binding protein (PB2)

Quercetin and its glycoside derivatives, such as quercetin 3'-glucuronide and quercetin-7-O-glucoside, effectively block the RNA polymerase (PB2) of influenza viruses by precisely occupying the mGTP binding site, resulting in the disruption of the viral life cycle<sup>41,42</sup>. Consistently, all putative flavonoids detected in the *C. mimosoides* extract exhibited a similar orientation pattern to those positive ligands (e.g., quercetin, mGTP and favipiravir-RTP) with binding scores ranging from 59.86 to 73.87 (Table 5; Fig. 13). Among them, two flavone glycosides—scutellarin and luteolin 7-glucuronide—demonstrated the highest binding affinities, scoring 73.69 and 73.87 in fitness scores, respectively. By utilizing the ring systems A and C, the former can generate H-bonds (2.38–2.5 Å) and hydrophobic interactions with Ser321, Phe323, His357, Phe363, Lys376, and Phe404. Meanwhile, its glucuronide moiety formed three H-bonds with Arg355 and Asn429 (1.70–2.99 Å) (Fig. 14). Likewise, luteolin 7-glucuronide, with logP value of 1.55, formed multiple robust hydrophobic interactions with the target residues,



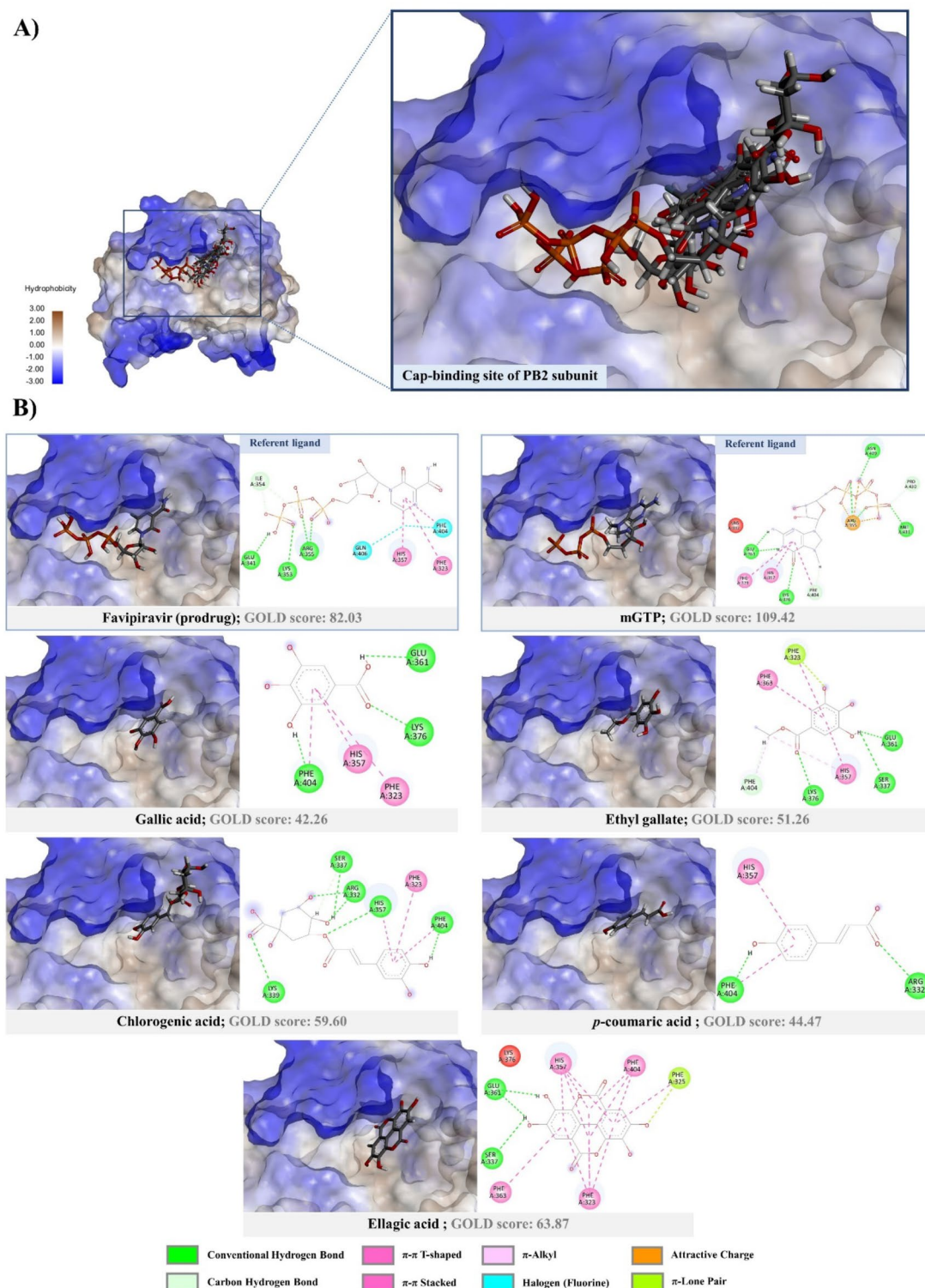


**Fig. 12.** (A) Structural orientation of phenolic substances and the two positive ligands —mGTP and favipiravir-RTP—in the cap-binding domain of PB2 subunit of influenza RNA polymerase. (B) Their specific interactions with the hydrophobic pocket.

where its glucosiduronic acid moiety revealed three H-bonds with Arg355 (2.43 Å) and Asn429 (1.64–2.91 Å). In light of our results, glycosylated flavonoids always exhibited greater binding energies over their aglycone scaffolds. For instance, the fitness scores of quercetin and its three derivatives decreased in order of substitution degree: Quercitrin (quercetin 3-rhamnoside: Q3R) > Guaijaverin (quercetin-3-O-arabinoside) > Taxifolin (dihydroquercetin) > Quercetin. Notably, quercitrin exhibited energy levels comparable to the reference ligand,

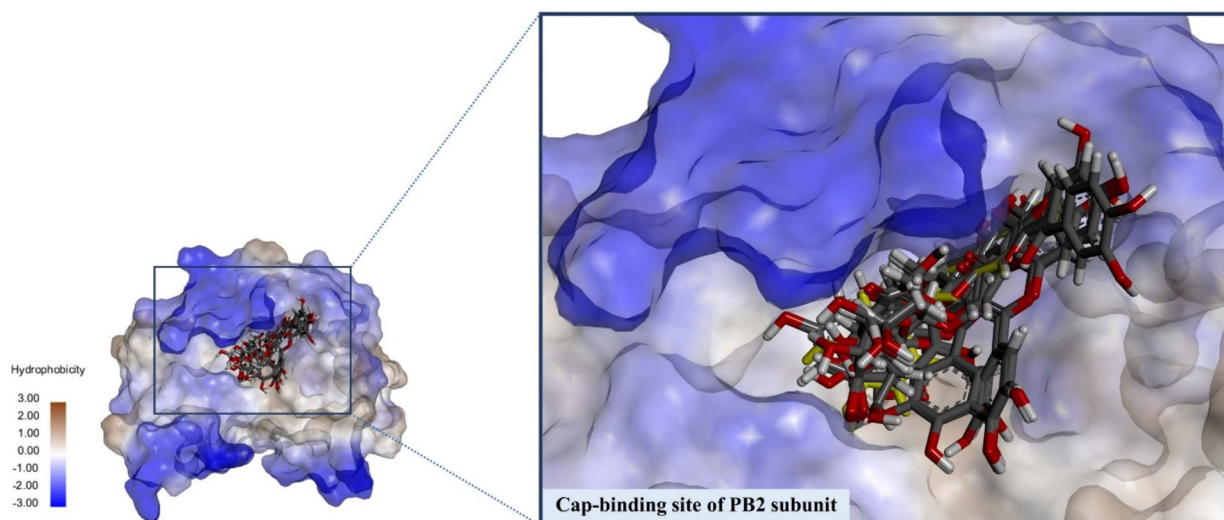


**Fig. 13.** Structural orientation of flavonoids and other glycoside analogues with the two positive ligands — mGTP and favipiravir-RTP—in the cap-binding domain of PB2 subunit of influenza RNA polymerase.

quercetin-7-O-glucoside, which is known to directly inhibit viral RNA polymerase by occupying the m7GTP binding site [35]. Q3R formed five strong H-bonds (1.69–2.92 Å) and engaged in six promising  $\pi$ -interactions with Phe404, Phe323, Phe363, and His357, suggesting it is well positioned in the target region. Following this pattern, myricitrin (myricetin 3-O-rhamnoside) exhibited superior binding property compared to its analogs—myricetin and dihydromyricetin—through seven hydrophobic contacts, alongside two H-bonds (1.74 to 2.28 Å). The rhamnoside moiety also enhanced stability by forming three H-bonds (1.98 to 2.97 Å) and three alkyl-bonds with Lys339, Arg355, Phe325, and Ser324 (3.98 to 4.88 Å) in the expected region. While the selective inhibition of myricitrin remains ambiguous, Sang et al.<sup>60</sup> demonstrated that its molecular scaffold—myricetin—significantly disrupts influenza A virus replication by occupying at PB2 subunit. Consequently, flavonoids that share the same biosynthetic origin, characterized by (C6-C3-C6) skeleton, including myricetin, dihydromyricetin, and even two glycosidic kaempferol derivatives (astragalin and afzelin) apparently active due to their more significant number of H-bonds and hydrophobic interactions with the mGTP recognition residues. Based on the basic flavonoid structure, catechin and galocatechin are likewise predicted to occupy PB2 subunit of influenza RNA polymerase, forming various hydrophobic interactions and hydrogen bonds with the key residues Phe323, His357, and Phe404 (Fig. 14). Despite further elucidation is needed, previous studies have found that plant extracts containing various catechins (e.g., (+)-catechin, ECGC, EGC, ECG, EC, and GCG) exert antiviral activity against flu viruses grown in MDCK cells by disrupting RNA synthesis in addition to the inhibitory effect on NA and HA proteins<sup>63</sup>.

#### Non-phenolic against PB2 (4NCE)

Germacone, a major component of the essential oil in *Rhizoma curcuma*, not only inhibits the early stages (e.g., entry and spreading) of the influenza life cycle but also disrupts the replication processes<sup>58</sup>. Here, we found that the putative germacone ( $m/z$  219.1393) interacted with the cap-binding site with energy levels similar to gallic acid (Fig. 15B). This cyclic sesquiterpene formed several strong intermolecular interactions with highly conserved residues including Phe323, Phe325, Arg355, His357, Phe363, Phe404, and Met431 (3.56 to 5.32 Å), suggesting its potential polypharmacological effects in addition to neuraminidase (Fig. 15B). Therefore, the inhibitory effects of dicarboxylic acids were postulated to be active due to the strong binding affinity (Table 5) and integral lipophilicity, with LogP values ranging from 1.44 to 2.98 (Table 3). Tetradecanedioic acid, for instance, established four promising H-bonds with Glu341 (1.94 Å), Lys353 (3.04 Å), Ile354 (2.78 Å), and Glu361 (2.02 Å), along with several hydrophobic interactions with the key residues (Phe404, His357, Pro430, Arg355, and Met351), highly similar to mGTP and favipiravir-RTP (Fig. 15A). Given the lack of evidence regarding the anti-influenza effects of longer-chain dicarboxylic acids, using alternative strategies, such as MD simulation, is crucial to prospectively assess stability in various complex structures.

## Conclusion

For the first time, we demonstrated that increasing the ethanol concentration to 30% (v/v) in the extraction solvent led to a substantial increase in the phytochemical profiling, antioxidant, and anti-influenza activities of the *C. mimosoides* hydroethanolic extract. Gallic acid could be a representative marker based on RP-HPLC analysis. After being characterized by UPLC-ESI(±)-QTOF-MS/MS and verified using multiple mass spectra annotation tools, simple phenolic acids and flavonoids were found to be predominant in the newly established plant extract. It exhibited potent anti-influenza activity, approximately 3.35 times higher than that of the aqueous extract, where flavonoids were barely detected. The absence of hemolytic activity indicates its potential use as a safe antiviral agent. Docking studies affirmed that gallic acid, ethyl gallate, ellagic acid, and chlorogenic acid,



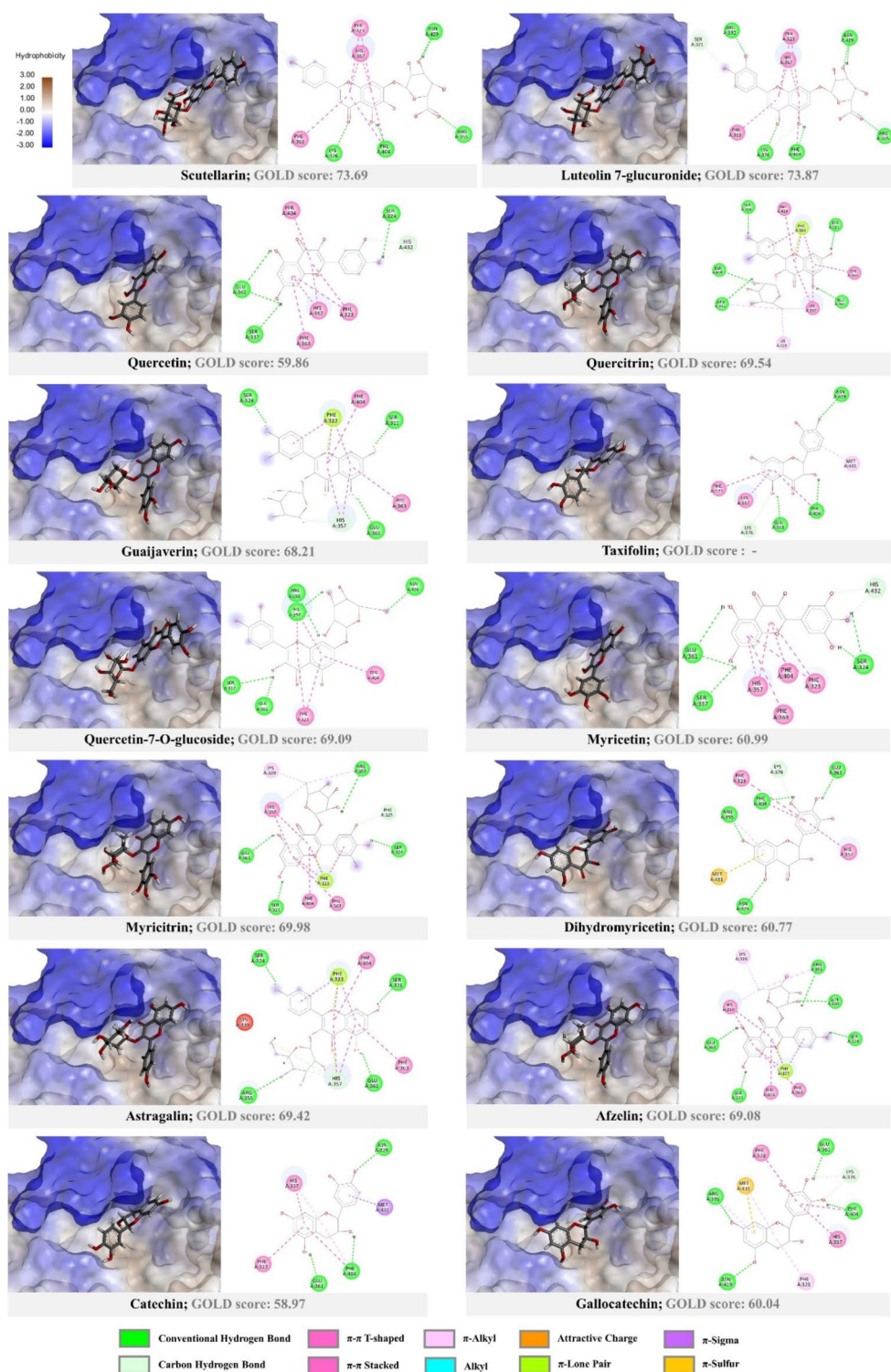


**Fig. 14.** Ligand-receptor interactions of polyphenols with the highly conserved hydrophobic residues of PB2 subunit. Their interactions with the hydrophobic pocket.

along with all flavonoids, interacted well with both NA and PB2, supporting the boosted antiviral activity. Molecular dynamics simulations and further in vitro assays are needed to underscore its potential uses. Owing to the higher lipophilicity of flavonoids, increasing the ratio of ethanol in the solvent used might lead to enhanced antiviral activity of the *C. mimosoides* aqueous-ethanolic extract in the long run.

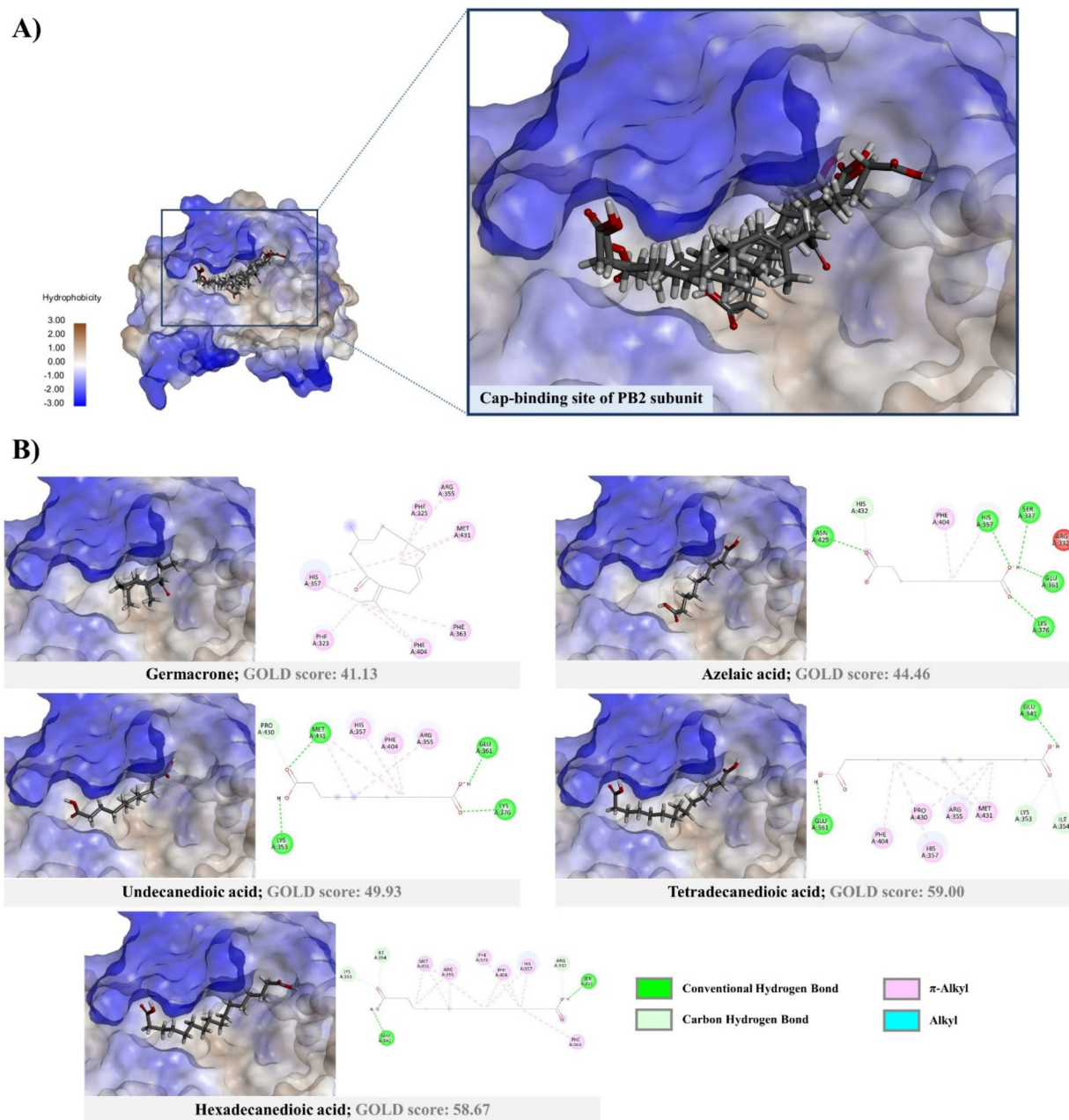


**Fig. 15.** (A) Non-phenolics substances predicted to structurally orientate in the cap-binding region of influenza A RNA polymerase (PB2). (B) Their interactions with the hydrophobic pocket.

### Data availability

The data that support the findings of this study are available from the corresponding author upon reasonable request. The data are not publicly available due to privacy and/or ethical restrictions.

Received: 13 August 2024; Accepted: 20 January 2025

Published online: 01 February 2025

### References

1. Mukhtar, M. et al. Antiviral potentials of medicinal plants. *Virus Res.* **131** (2), 111–120. <https://doi.org/10.1016/j.virusres.2007.09.008> (2008).
2. Siddiqui, M. H. et al. A mini-review of anti-hepatitis B virus activity of medicinal plants. *Biotechnol. Biotechnol. Equip.* **31** (1), 9–15. <https://doi.org/10.1080/13102818.2016.1240593> (2017).
3. Ganjhu, R. K. et al. Herbal plants and plant preparations as remedial approach for viral diseases. *Virusdisease* **26**, 225–236. <https://doi.org/10.1007/s13337-015-0276-6> (2015).
4. Chojnacka, K. et al. Antiviral properties of polyphenols from plants. *Foods* **10** (10), 2277. <https://doi.org/10.3390/foods10102277> (2021).

5. Yang, Z. F. et al. Comparison of in vitro antiviral activity of tea polyphenols against influenza A and B viruses and structure–activity relationship analysis. *Fitoterapia* **93**, 47–53. <https://doi.org/10.1016/j.fitote.2013.12.011> (2014).
6. Badshah, S. L. et al. Antiviral activities of flavonoids. *Biomed. Pharmacother.* **140**, 111596. <https://doi.org/10.1016/j.biopha.2021.111596> (2021).
7. You, H. L., Chen, C. J., Eng, H. L., Liao, P. L. & Huang, S. T. The effectiveness and mechanism of *Toona sinensis* extract inhibit attachment of pandemic influenza A (H1N1) virus. *Evid. Based Complement. Altern. Med.* **2013** (1), 479718. <https://doi.org/10.1155/2013/479718> (2013).
8. You, H. L. et al. Anti-pandemic influenza A (H1N1) virus potential of catechin and gallic acid. *J. Chin. Med. Assoc.* **81** (5) 458–68. <https://doi.org/10.1016/j.jcma.2017.11.007> (2018).
9. Zhao, M. et al. Traditional uses, chemical constituents and pharmacological activities of the *Toona sinensis* plant. *Molecules* **29** (3), 718. <https://doi.org/10.3390/molecules29030718> (2024).
10. Park, S. et al. *Aronia melanocarpa* and its components demonstrate antiviral activity against influenza viruses. *Biochem. Biophys. Res. Commun.* **440** (1), 14–19. <https://doi.org/10.1016/j.bbrc.2013.08.090> (2013).
11. Devi, A. B. & Sarala, R. Substantial effect of phytochemical constituents against the pandemic disease influenza—a review. *Future J. Pharm. Sci.* **7** (1), 120. <https://doi.org/10.1186/s43094-021-00269-5> (2021).
12. Rangsinth, P. et al. Leaf extract of *Caesalpinia mimosoides* enhances oxidative stress resistance and prolongs lifespan in *Caenorhabditis elegans*. *BMC Complement. Altern. Med.* **19**, 1–3. <https://doi.org/10.1186/s12906-019-2578-5> (2019).
13. Bhat, P., Upadhy, V., Hegde, G. R., Hegde, H. V. & Roy, S. Attenuation of dermal wounds through topical application of ointment containing phenol enriched fraction of *Caesalpinia mimosoides* Lam. *Front. Pharmacol.* **13**, 1025848. <https://doi.org/10.3389/fphar.2022.1025848> (2022).
14. Adisak, P., Temduang, L. & Patcharee, B. Cytotoxic effects of phytophenolics from *Caesalpinia mimosoides* Lamkon cervical carcinoma cell lines through an apoptotic pathway. *Asian Pac. J. Cancer Prev.* **15**, 449–454. <https://doi.org/10.7314/APJCP.2014.15.1.449> (2014).
15. Klamrak, A. et al. Unveiling the potent antiviral and antioxidant activities of an aqueous extract from *Caesalpinia mimosoides* Lamk: Cheminformatics and molecular docking approaches. *Foods* **13** (1) 81. <https://doi.org/10.3390/foods13010081> (2023).
16. Oh, M., Park, S., Song, J. H., Ko, H. J. & Kim, S. H. Chemical components from the twigs of *Caesalpinia latisiliqua* and their antiviral activity. *J. Nat. Med.* **74**, 26–33. <https://doi.org/10.1007/s11418-019-01335-2> (2020).
17. Kiselova-Kaneva, Y., Galunska, B., Nikolova, M., Dincheva, I. & Badjakov, I. High resolution LC-MS/MS characterization of polyphenolic composition and evaluation of antioxidant activity of *Sambucus ebulus* fruit tea traditionally used in Bulgaria as a functional food. *Food Chem.* **367**, 130759. <https://doi.org/10.1016/j.foodchem.2021.130759> (2022).
18. Wille, S. M. et al. Liquid chromatography high-resolution mass spectrometry in forensic toxicology: what are the specifics of method development, validation and quality assurance for comprehensive screening approaches? *Curr. Pharm. Design* **28** (15), 1230–1244. <https://doi.org/10.2174/1381612828666220526152259> (2022).
19. Dührkop, K., Shen, H., Meusel, M., Rousu, J. & Böcker, S. Searching molecular structure databases with tandem mass spectra using CSI: FingerID. *Proc. Natl. Acad. Sci.* **112** (41), 12580–12585. <https://doi.org/10.1073/pnas.1509788111> (2015).
20. Ruttkies, C., Schymanski, E. L., Wolf, S., Hollender, J. & Neumann, S. MetFrag relaunched: incorporating strategies beyond in silico fragmentation. *J. Cheminform.* **8**, 1–6. <https://doi.org/10.1186/s13321-016-0115-9> (2016).
21. Dührkop, K. et al. SIRIUS 4: a rapid tool for turning tandem mass spectra into metabolite structure information. *Nat. Methods* **16** (4), 299–302. <https://doi.org/10.1038/s41592-019-0344-8> (2019).
22. Dührkop, K. et al. Systematic classification of unknown metabolites using high-resolution fragmentation mass spectra. *Nat. Biotechnol.* **39** (4), 462–471. <https://doi.org/10.1038/s41587-020-0740-8> (2021).
23. Wang, Q. et al. Protocatechuic acid protects mice from influenza a virus infection. *Eur. J. Clin. Microbiol. Infect. Dis.* **41** (4), 589–596. <https://doi.org/10.1007/s10096-022-04401-y> (2022).
24. Wang, S. et al. Integration of LC/MS-based molecular networking and molecular docking allows in-depth annotation and prediction of the metabolome: a study of *Salvia miltiorrhiza* Bunge. *Ind. Crops Prod.* **186**, 115298. <https://doi.org/10.1016/j.indcro.2022.115298> (2022).
25. Bhattacharai, K. et al. Bioprospecting the metabolome of plant *Urtica dioica* L.: a fast dereplication and annotation workflow in plant metabolomics. *Evid. Based Complement. Altern. Med.* **2022** (1), 3710791. <https://doi.org/10.1155/2022/3710791> (2022).
26. Blaženović, I., Kind, T., Ji, J. & Fiehn, O. Software tools and approaches for compound identification of LC-MS/MS data in metabolomics. *Metabolites* **8** (2), 31. <https://doi.org/10.3390/metabo8020031> (2018).
27. Rattanata, N. et al. Inhibitory effects of gallic acid isolated from *Caesalpinia mimosoides* Lamk on cholangiocarcinoma cell lines and foodborne pathogenic Bacteria. *Asian Pac. J. Cancer Prev.* **17** (3), 1341–1345. <https://doi.org/10.7314/APJCP.2016.17.3.1341> (2016).
28. Falcone Ferreyra, M. L., Rius, S. P. & Casati, P. Flavonoids: biosynthesis, biological functions, and biotechnological applications. *Front. Plant Sci.* **3**, 222. <https://doi.org/10.3389/fpls.2012.00222> (2012).
29. Mehrbod, P. et al. Quercetin as a natural therapeutic candidate for the treatment of influenza virus. *Biomolecules* **11** (1), 10. <https://doi.org/10.3390/biom11010010> (2020).
30. Kanehisa, M. & Goto, S. Kyoto encyclopedia of genes and genomes. *Nucleic Acids Res.* **28** (1), 27–30. <https://doi.org/10.1093/nar/28.1.27> (2000).
31. Kanehisa, M. Toward understanding the origin and evolution of cellular organisms. *Protein Sci.* **28** (11), 1947–1951. <https://doi.org/10.1002/pro.3715> (2019).
32. Zohra, M. & Fawzia, A. Hemolytic activity of different herbal extracts used in Algeria. *Int. J. Pharma Sci. Res.* **5** (8), 495–500. <https://www.ijpsr.info/docs/IJPSR14-05-08-010> (2014).
33. Du, R., Cui, Q. & Rong, L. Competitive cooperation of hemagglutinin and neuraminidase during influenza a virus entry. *Viruses* **11** (5), 458. <https://doi.org/10.3390/v11050458> (2019).
34. Liu, Z. et al. Computational screen and experimental validation of anti-influenza effects of quercetin and chlorogenic acid from traditional Chinese medicine. *Sci. Rep.* **6** (1) 19095, (2016).
35. A.F., El-Sayed. Phytochemical profiling, antiviral activities, molecular docking, and dynamic simulations of selected *Ruellia* species extracts. *Sci. Rep.* **14** (1), 15381 (2024).
36. Zhang, T. et al. Anti-influenza virus phytochemicals from radix paeoniae alba and characterization of their neuraminidase inhibitory activities. *J. Ethnopharmacol.* **253**, 112671. <https://doi.org/10.1016/j.jep.2020.112671> (2020).
37. Wu, S., Chen, W., Lu, S., Zhang, H. & Yin, L. Metabolic engineering of shikimic acid biosynthesis pathway for the production of shikimic acid and its branched products in microorganisms: advances and prospects. *Molecules* **27** (15), 4779. <https://doi.org/10.3390/molecules27154779> (2022).
38. Tock, M. L. et al. Exploring the phytochemical variation of non-volatile metabolites within three South African salvia species using UPLC-MS fingerprinting and chemometric analysis. *Fitoterapia* **152**, 104940. <https://doi.org/10.1016/j.fitote.2021.104940> (2021).
39. Yan, L., Yin, P., Ma, C. & Liu, Y. Method development and validation for pharmacokinetic and tissue distributions of ellagic acid using ultrahigh performance liquid chromatography–tandem mass spectrometry (UPLC-MS/MS). *Molecules* **19** (11), 18923–18935. <https://doi.org/10.3390/molecules191118923> (2014).
40. Wu, W. et al. Quercetin as an antiviral agent inhibits influenza a virus (IAV) entry. *Viruses* **8** (1), 6. <https://doi.org/10.3390/v8010006> (2015).



41. Gansukh, E., Kazibwe, Z., Pandurangan, M., Judy, G. & Kim, D. H. Probing the impact of quercetin-7-O-glucoside on influenza virus replication influence. *Phytomedicine* **23** (9), 958–967. <https://doi.org/10.1016/j.phymed.2016.06.001> (2016).
42. Gansukh, E., Nile, A., Kim, D. H., Oh, J. W. & Nile, S. H. New insights into antiviral and cytotoxic potential of quercetin and its derivatives—a biochemical perspective. *Food Chem.* **334**, 127508. <https://doi.org/10.1016/j.foodchem.2020.127508> (2021).
43. Mandal, S. K. & Munshi, P. Predicting accurate lead structure for screening molecular libraries: a quantum crystallographic approach. *Molecules* **26** (9), 2605. <https://doi.org/10.3390/molecules26092605> (2021).
44. Tang, C. et al. Polyphenol rich sugarcane extract (PRSE) has potential antiviral activity against influenza a virus in vitro. *Virology* **590**, 109969. <https://doi.org/10.1016/j.virol.2023.109969> (2024).
45. Di Petrillo, A., Orrù, G., Fais, A. & Fantini, M. C. Quercetin and its derivatives as antiviral potentials: a comprehensive review. *Phytother. Res.* **36** (1), 266–278. <https://doi.org/10.1002/ptr.7309> (2022).
46. Pokharkar, O., Anumolu, H., Zyryanov, G. V. & Tsurkan, M. V. Natural products from red algal genus *Laurencia* as potential inhibitors of RdRp and nsp15 enzymes of SARS-CoV-2: an in silico perspective. *Microbiol. Res.* **14** (3), 1020–1048. <https://doi.org/10.3390/microbiolres14030069> (2023).
47. Sadati, S. M., Gheibi, N., Ranjbar, S. & Hashemzadeh, M. S. Docking study of flavonoid derivatives as potent inhibitors of influenza H1N1 virus neuraminidase. *Biomed. Rep.* **10** (1), 33–38. <https://doi.org/10.3892/br.2018.1173> (2019).
48. Lee, M. M. et al. The antiviral activity of *Thuja orientalis* folium against influenza A virus. *Virus Res.* **335**, 199199. <https://doi.org/10.1016/j.virusres.2023.199199> (2023).
49. McAuley, J. L., Gilbertson, B. P., Trifkovic, S., Brown, L. E. & McKimm-Breschkin, J. L. Influenza virus neuraminidase structure and functions. *Front. Microbiol.* **10**, 39. <https://doi.org/10.3389/fmicb.2019.00039> (2019).
50. Motlhatlego, K. E., Abdalla, M. A., Leonard, C. M., Eloff, J. N. & McGaw, L. J. Inhibitory effect of Newtonia extracts and myricetin-3-o-rhamnoside (myricitrin) on bacterial biofilm formation. *BMC Complement. Med. Ther.* **20**, 1–10. <https://doi.org/10.1186/s12906-020-03139-4> (2020).
51. Ide, K., Kawasaki, Y., Kawakami, K. & Yamada, H. Anti-influenza virus effects of catechins: a molecular and clinical review. *Curr. Med. Chem.* **23** (42), 4773–4783. <https://www.ingentaconnect.com/content/ben/cmc/2016/00000023/00000042/art00005> (2016).
52. Furushima, D., Ide, K. & Yamada, H. Effect of tea catechins on influenza infection and the common cold with a focus on epidemiological/clinical studies. *Molecules* **23** (7), 1795. <https://doi.org/10.3390/molecules23071795> (2018).
53. Fechter, P. et al. Two aromatic residues in PB2 subunit of influenza A RNA polymerase are crucial for cap binding. *J. Biol. Chem.* **278** (22), 20381–20388. <https://doi.org/10.1074/jbc.M300130200> (2003).
54. Ding, Y. et al. Antiviral activity of chlorogenic acid against influenza A (H1N1/H3N2) virus and its inhibition of neuraminidase. *Sci. Rep.* **7** (1), 45723. <https://doi.org/10.1038/srep45723> (2017).
55. Muchtaridi, M. et al. Decaffeination and neuraminidase inhibitory activity of arabica green coffee (*Coffea arabica*) beans: chlorogenic acid as a potential bioactive compound. *Molecules* **26** (11), 3402. <https://doi.org/10.3390/molecules26113402> (2021).
56. Kai, H. et al. In vitro and in vivo anti-influenza virus activities of flavonoids and related compounds as components of *Brazilian propolis* (AF-08). *J. Funct. Foods* **8**, 214–223. <https://doi.org/10.1016/j.jff.2014.03.019> (2014).
57. Gramza-Michałowska, A., Sidor, A. & Kulczyński, B. Berries as a potential anti-influenza factor—A review. *J. Funct. Foods* **37**, 116–137. <https://doi.org/10.1016/j.jff.2017.07.050> (2017).
58. Liao, Q., Qian, Z., Liu, R., An, L. & Chen, X. Germacrone inhibits early stages of influenza virus infection. *Antiviral Res.* **100** (3), 578–588. <https://doi.org/10.1016/j.antiviral.2013.09.021> (2013).
59. Moradi, M. T., Karimi, A., Shahrani, M., Hashemi, L. & Ghaffari-Goosheh, M. S. Anti-influenza virus activity and phenolic content of pomegranate (*Punica granatum* L.) peel extract and fractions. *Avicenna J. Med. Biotechnol.* **11** (4), 285. <https://www.ncbi.nlm.nih.gov/pmc/articles/PMC6925405> (2019).
60. Sang, H. et al. Multiple modes of action of myricetin in influenza a virus infection. *Phytother. Res.* **35** (5), 2797–2806. <https://doi.org/10.1002/ptr.7025> (2021).
61. Luo, X. et al. Computational study of the molecular mechanism of *Lonicera japonica* organic acids against influenza. *Tradition. Med. Res.* **1** (3), 128–137. <https://doi.org/10.53388/TMR201603018> (2016).
62. Kumari, R. et al. Sambhara. Antiviral approaches against influenza virus. *Clin. Microbiol. Rev.* **36** (1), e0004022. <https://doi.org/10.1128/cmr.00040-22> (2023).
63. Kuzuhara, T., Iwai, Y., Takahashi, H., Hatakeyama, D. & Echigo, N. Green tea catechins inhibit the endonuclease activity of influenza a virus RNA polymerase. *PLoS Curr.* **1** <https://doi.org/10.1371/currents.RRN1052> (2009).

## Acknowledgements

The authors are extremely grateful to the Faculty of Pharmaceutical Sciences, Khon Kaen University, Thailand.

## Author contributions

S.D., A.K., S.T., P.S., N.J., S.K., K.C., R.P., A.C., J.D.: conceptualization. A.K., N.N., J.N., Jaran. N., P.J., Y.S., T.S., S.S.: methodology. A.K., P.J.: software. S.D., A.K.: validation. A.K., S.S.R., N.N.: formal analysis. A.K., S.S.R., J.N., Jaran. N., P.J., Y.S., T.S., J.D.: investigation. S.T.: resources. A.K., N.N., J.N., Jaran. N., P.J., Y.S., K.C.: data curation. S.S.R., A.K.: writing—original draft preparation. A.K., S.S.R.: writing—review and editing. A.K., S.S.R., N.N.: visualization. S.D.: supervision, project administration and funding acquisition. All authors have read and agreed to the published version of the manuscript.

## Funding

This research was funded by the Program Management Unit for Human Resources and Institutional Development, Research and Innovation (PMU-B) for postdoctoral scholarship [PMU-B grant number: B13F660069]. It received partial funding from The Fundamental Fund of Khon Kean University (KKU), which received financial support from the National Science, Research and Innovation Fund (NSRF), Thailand. The research was supported by NSRF under the Basic Research Fund of Khon Kaen University.

## Declarations

## Competing interests

The authors declare no competing interests.

## Additional information

**Correspondence** and requests for materials should be addressed to S.D.

**Reprints and permissions information** is available at [www.nature.com/reprints](http://www.nature.com/reprints).

**Publisher's note** Springer Nature remains neutral with regard to jurisdictional claims in published maps and institutional affiliations.

**Open Access** This article is licensed under a Creative Commons Attribution-NonCommercial-NoDerivatives 4.0 International License, which permits any non-commercial use, sharing, distribution and reproduction in any medium or format, as long as you give appropriate credit to the original author(s) and the source, provide a link to the Creative Commons licence, and indicate if you modified the licensed material. You do not have permission under this licence to share adapted material derived from this article or parts of it. The images or other third party material in this article are included in the article's Creative Commons licence, unless indicated otherwise in a credit line to the material. If material is not included in the article's Creative Commons licence and your intended use is not permitted by statutory regulation or exceeds the permitted use, you will need to obtain permission directly from the copyright holder. To view a copy of this licence, visit <http://creativecommons.org/licenses/by-nc-nd/4.0/>.

© The Author(s) 2025